TABLE III – MULTIVARIATE COX REGRESSION ANALYSIS OF THE FACTORS ASSOCIATED WITH SURVIVAL

Step	Variable	Relative risk (95% CI)	p (log-rank)
The first	Age (yr)		0.0499
	0–19	1.040 (0.226–4.790)	0.9600
	20–39		
	40–59[1]	1.049 (0.404–2.719)	0.9220
	60+	3.073 (1.173–8.048)	0.0223
	Tumor histology		<0.0001
	Low-grade astrocytoma[1]		
	AA	3.673 (0.636–21.207)	0.0208
	GBM	13.894 (4.287–45.028)	<0.0001
	LAT1		0.0059
	(+)	0.179 (0.062–0.516)	0.0014
	(++)	0.405 (0.167–0.982)	0.0455
	(+++)[1]		
	4F2hc		0.4627
	(+)	1.455 (0.614–3.451)	0.3945
	(++)	0.925 (0.358–2.391)	0.8714
	(+++)[1]		
	Gender		
	Male	1.578 (0.764–3.260)	0.2180
	Female[1]		
	PCNA (%)		0.7026
	<5	0.376 (0.248–2.186)	0.5813
	5–30	0.755 (0.384–1.483)	0.4139
	>30[1]		
The final	Age (yr)		0.0244
	0–19	0.824 (0.192–3.538)	0.7948
	20–39[1]		
	40–59	0.951 (0.377–2.402)	0.9159
	60+	2.990 (1.162–7.697)	0.0231
	Tumor histology		<0.0001
	Low-grade astrocytoma[1]		
	AA	4.153 (1.305–13.218)	0.0159
	GBM	11.310 (3.819–33.495)	<0.0001
	LAT1		0.0004
	(+)	0.167 (0.065–0.430)	0.0002
	(++)	0.303 (0.139–0.660)	0.0026
	(+++)[1]		

CI, confidence interval.
[1]Reference category.–[2]Potential prognostic factors selected from Table II were used.

increased in number and the $OD_{595-655}$ value at day 5 showed more than 1.0. In contrast, almost complete suppression of the cell growth was observed when 25 mM BCH was added to the culture medium. When BCH was added at a concentration of more than 25 mM, cell survival was disturbed and a decrease in the $OD_{595-655}$ value was observed. BCH at a concentration of 1–10 mM revealed a limited effect. We confirmed that this growth inhibitory effect of the BCH on C6 glioma cells was not due to high osmolarity of the BCH-added culture medium since addition of the equivalent molarity of D-mannitol showed no remarkable effect on the growth of C6 glioma cells (data not shown).

Effects of BCH on tumor sizes in vivo *and on survival of rats after tumor inoculation*

The volume of tumor averaged 77.9 ± 16.7 mm^3 in Group 1 (n = 9) (BCH230/1 day), 146.8 ± 21.4 mm^3 in Group 2 (n = 9) (saline/1 day), 95.3 ± 13.6 mm^3 in Group 3 (n = 7) (BCH230/8 days), 109.9 ± 12.1 mm^3 in Group 4 (n = 12) (BCH50/8 days), 144.7 ± 19.1 mm^3 in Group 5 (n = 7) (saline/8 days), and 130.1 ± 21.8 mm^3 in Group 6 (n = 7) (mannitol50/8 days), respectively (mean ± SE) (Fig. 5). The volume of tumor in Group 1 was significantly smaller than that in Group 2 (p = 0.022). The volume of tumor in Group 3 was also smaller than that in Group 5, but the difference was not significant (p = 0.057). All animals lost weight within 6–17 days after tumor inoculation and continuously lost it thereafter. The time point of maximal body weight was significantly prolonged in the animals treated with 230 mM of BCH (Group 1) when compared with that of Group 2 (p = 0.026). Kaplan-Meier survival data of rats in Group 1 were significant (Fig. 6), compared to that of rats in Group 2 (p = 0.016 log-rank). BCH, saline or D-mannitol administration to a concentration of 50–230 mM was not associated with occurrence of seizures, or changes in behavior (such as sluggishness or inability to eat) in rats without tumor cells. The percentage of PCNA-positive cells in Group 1 was significantly smaller than that in Group 2 (p = 0.0182).

Discussion

We have demonstrated for the first time that high LAT1 immunostaining predicts a poor prognosis in patients with astrocytic brain tumors in general and in patients with GBM or low grade astrocytoma in particular. However, LAT1 was the second strongest predictor of outcome in general. It is speculated that LAT1 expression is upregulated so as to provide cells with essential amino acids for high levels of protein synthesis associated with cell activation and also to support rapid growth or continuous proliferation. Indeed, we found that high LAT1 expression correlated with high proliferating potential of the tumor estimated by PCNA immunohistochemistry. LAT1 also corresponds to TA1, an oncofetal antigen that is expressed primarily in fetal tissues and cancer cells.[10] A high level of LAT1 expression was also detected in human tumor cell lines such as stomach signet ring cell carcinoma (KATOIII), malignant melanoma (G-361), and lung small-cell carcinoma (RERF-LC-MA) by Northern blot analysis.[3] The database search indicated that partial or incomplete sequences of LAT1 (E16, TA1 and ASUR4b) were already reported.[5,6,11] E16 and ASUR4b were identified to be up-regulated upon the mitogenic stimulation of lymphocytes and the stimulation of A6 epithelial cell line by aldosterone, respectively,[5,11] suggesting highly regulated nature of LAT1 gene expression. TA1 was identified as

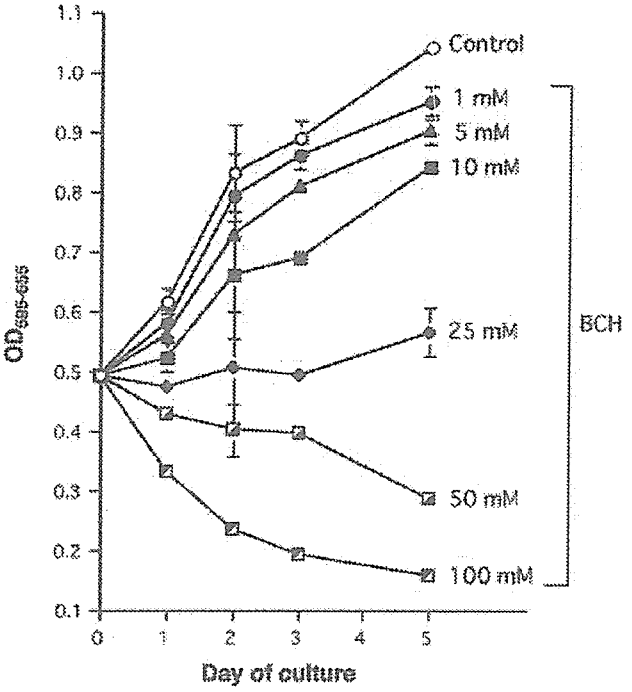

FIGURE 4 – Effect of the various concentration of BCH (from 1 to 100 mM) on the survival of C6 glioma cells was serially observed by MTT assay.

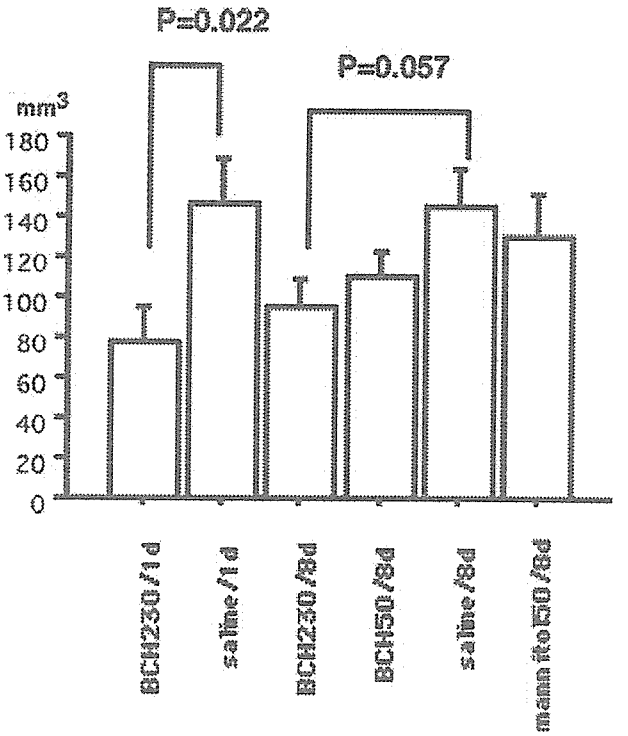

FIGURE 5 – Average tumor volumes ± SE in each group are shown. Fifty-one rats were divided into 6 experimental groups. Group 1 (BCH230/1 day) (n = 9) were given 230 mM of BCH 1 day after tumor inoculation. Group 2 (saline/1 day) (n = 9) were given the saline 1 day after tumor inoculation. In group 3 (BCH230/8 days) (n = 7), animals were given 230 mM of BCH 8 days after tumor inoculation. Group 4 (BCH50/8 days) (n = 12) received 50 mM of BCH 8 days after tumor inoculation. Group 5 (saline/8 days) (n = 7) were given the saline 8 days after tumor inoculation. Group 6 (mannitol50/8 days) (n = 7) were given 50 mM D-mannitol 8 days after tumor inoculation. Statistical significance was determined by ANOVA followed by Bonferroni/Dunn test.

a tumor-associated sequence with the oncofetal pattern of expression in rat liver.[6] TA1 immunoreactivity was abundant in human colon cancer *in vivo* but barely detected in surrounding normal colon tissue,[12] confirming the high level of expression of LAT1 protein in tumor cells. The 4F2hc is thought to be involved in the trafficking and regulation of system L neutral amino acid transport in mammalian cells as mentioned previously. Because 4F2hc is essential for LAT1 to be functional, the level of 4F2hc expression would greatly affect the formation of functional system L transporters in the plasma membrane. We found that high 4F2hc immunoreactivity also correlated with high LAT1 expression; however, LAT1 staining had a major impact on survival rate. Involvement of LAT1 in tumor progression is also strongly suggested by a recent study that showed that up-regulation of the CD98 complex, but not the CD98 heavy chain (4F2hc) alone, in Balb3T3 cells resulted in tumorigenicity in nude mice.[13] LAT1 has been shown to be a transiently expressed membrane protein with the rapid degradation signal AUUUA.[5] Nakamura *et al.* demonstrated that LAT1 is expressed minimally at the plasma membrane in cancer cells, remaining mostly in the Golgi area, and requires 4F2hc to be sorted to the cell surface.[14] The immunoreactivity of LAT1 in the plasma membrane may represent its function. We did not differentiate the immunoreactivity of both cytosol and plasma membrane when estimating the grade of immunoreactivity of LAT1. However, the overall immunoreactivity for LAT1 did correlate well with the prognosis of patients with astrocytic tumors. Cytoplasmic LAT1 immunoreactivity may represent an intracellular pool of LAT1, and may correlate with the biological activity of cells.

To clarify the role of LAT1 in glioma cells, we tested a relatively specific inhibitor to LAT1, BCH, and found that BCH suppressed strongly C6 glioma cell growth *in vitro*. In addition, BCH also inhibited mortality of rats treated with C6 glioma cells. BCH at a concentration of 25 mM showed no significant effect on normal human astrocytes *in vitro* (data not shown). BCH is a nonmetabolizable artificial amino acid and a transportable inhibitor for LAT1. Yanagida *et al.* showed that a high-affinity substrate, leucine, and a low-affinity substrate, glutamine, but not a nonsubstrate, alanine, were effluxed *via* LAT1 by the application of leucine in the medium, confirming that LAT1 is an amino acid exchanger.[15] This, furthermore, suggests that the substrate selectivity of the intracellular substrate binding site of LAT1 is similar to that of the extracellular substrate binding site. Amino acids are released *via* LAT1 in exchange for the influx of amino acids; thus, no net amino acid influx should be observed. Glutamine, which is abundantly present in cells and generated intracellularly, is transported by LAT1 albeit with low affinity, consistent with a previous report for *Xenopus* LAT1.[4] Yanagida *et al.* further demonstrated that intracellularly loaded glutamine is effluxed in exchange for extracellularly applied leucine.[15] Therefore, they propose that extracellular high-affinity LAT1 substrates, most of which are essential amino acids, are taken up by cells *via* LAT1 driven by the exchange for intracellular-glutamine, which results in the net influx of essential amino acids.[15] An interesting finding of the Northern blot analysis of the tumor cell line is that the expression level of 4F2hc is quite varied among tumor cell lines, particularly in leukemia cell lines.[15] Yanagida *et al.* found 3 leukemia cell lines in which 4F2hc messages were not detected.[15] In those cell lines that lack 4F2hc expression, LAT1 was still expressed, suggesting different mechanisms of regulation in LAT1 and 4F2hc gene expression. Consistent with this, it was shown that LAT1 and 4F2hc respond differently to amino acid availability in rat hepatic cells.[16]

Several clinical investigations demonstrated the significant relation of the uptake of radiolabeled amino acid in gliomas and proliferation, biological aggressiveness or histological grading of

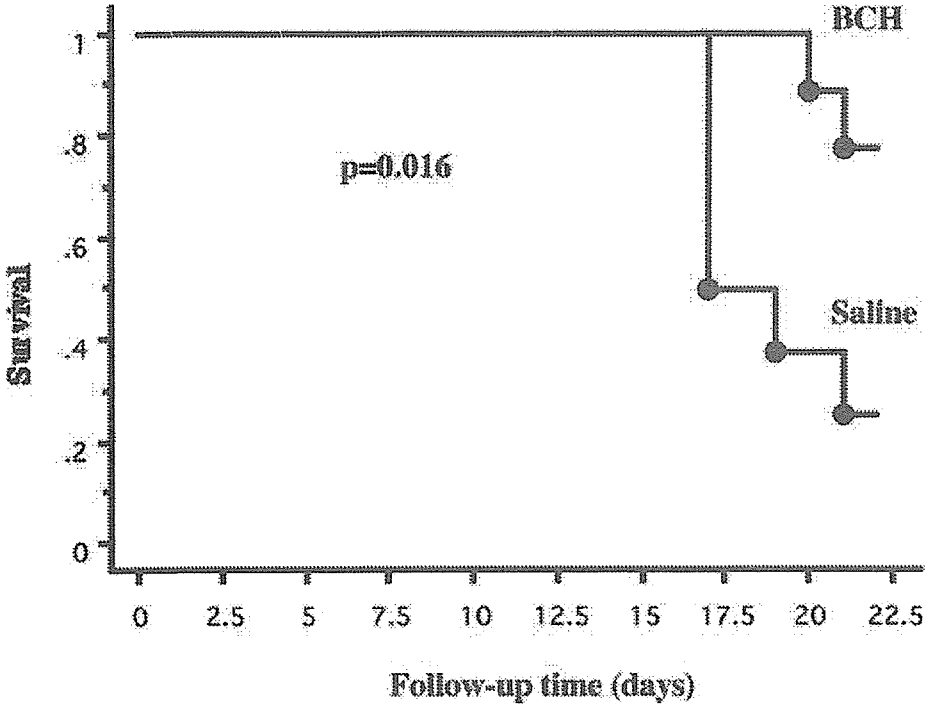

FIGURE 6 – Kaplan-Meier survival curves of C6 glioma-bearing rats after implantation of tumor cells.

these tumors.[17,18] A significant correlation of iodine-123–methyltyrosine (IMT) uptake in gliomas and the expression of the proliferation marker Ki-67 has been reported.[18] Recent studies also demonstrated significant longer survival times in patients with cerebral gliomas with low amino acid uptake than in gliomas with high amino acid uptake.[19] The results of this study support the hypothesis that the uptake of radiolabeled amino acids such as IMT is dependent on the proliferative activity of human gliomas. It is noteworthy that in cultured human glioma cells, membrane transport of IMT is dominated by BCH-sensitive transport system, LAT1.[20,21] LAT1-mediated IMT transport and 4F2 antigen expression are dependent on proliferation rate of human glioma cells *in vitro* and are significantly correlated to each other.[20] These data give further support to the involvement of the LAT1 in cell proliferation.[20,22] Thompson and coworkers recently reported the role of LAT1 as a potential therapeutic target in hepatic tumor cells *in vitro*.[23]

The present study suggests that LAT1 may play an important role in human high-grade gliomas. In addition, inhibitors to LAT1 may be an effective therapeutic option for high-grade gliomas.

References

1. Shrieve DC, Alexander E, III, Black PM, Wen PY, Fine HA, Kooy HM, Loeffler JS. Treatment of patients with primary glioblastoma multiforme with standard postoperative radiotherapy and radiosurgical boost: prognostic factors and long-term outcome. J Neurosurg 1999;90:72–7.
2. Millauer B, Shawver LK, Plate KH, Risau W, Ullrich A. Glioblastoma growth inhibited in vivo by a dominant-negative Flk-1 mutant. Nature 1994;367:576–9.
3. Kanai Y, Segawa H, Miyamoto K, Uchino H, Takeda E, Endou H. Expression cloning and characterization of a transporter for large neutral amino acids activated by the heavy chain of 4F2 antigen (CD98). J Biol Chem 1998;273:23629–32.
4. Mastroberardino L, Spindler B, Pfeiffer R, Skelly PJ, Loffing J, Shoemaker CB, Verrey F. Amino-acid transport by heterodimers of 4F2hc/CD98 and members of a permease family. Nature 1998;395:288–91.
5. Gaugitsch HW, Prieschl EE, Kalthoff F, Huber NE, Baumruker T. A novel transiently expressed, integral membrane protein linked to cell activation. Molecular cloning via the rapid degradation signal AUUUA. J Biol Chem 1992;267:11267–73.
6. Sang J, Lim YP, Panzica M, Finch P, Thompson NL. TA1, a highly conserved oncofetal complementary DNA from rat hepatoma, encodes an integral membrane protein associated with liver development, carcinogenesis, and cell activation. Cancer Res 1995;55:1152–9.
7. Bruce JN, Falavigna A, Johnson JP, Hall JS, Birch BD, Yoon JT, Wu EX, Fine RL, Parsa AT. Intracerebral clysis in a rat glioma model. Neurosurgery 2000;46:683–91.
8. Kleihues P, Cavenee WK. Pathology and genetics of tumours of the nervous system. Lyon, France: IARC, 2000. p 6.
9. Chairoungdua A, Segawa H, Kim JY, Miyamoto K, Haga H, Fukui Y, Mizoguchi K, Ito H, Takeda E, Endou H, Kanai Y. Identification of an amino acid transporter associated with the cystinuria-related type II membrane glycoprotein. J Biol Chem 1999;274:28845–8.
10. Mannion BA, Kolesnikova TV, Lin SH, Wang S, Thompson NL, Hemler ME. The light chain of CD98 is identified as E16/TA1 protein. J Biol Chem 1998;273:33127–9.
11. Spindler B, Mastroberardino L, Custer M, Verrey F. Characterization of early aldosterone-induced RNAs identified in A6 kidney epithelia. Pflugers Arch 1997;434:323–31.
12. Wolf DA, Wang S, Panzia MA, Bassily NH, Thompson NL. Expression of a highly conserved oncofetal gene, TA1/E16, in human colon carcinoma and other primary cancers: homology to *Schistosoma mansoni* amino acid permease and *Caenorhabditis elegans* gene products. Cancer Res 1996;56:5012–22.
13. Shishido T, Uno S, Kamohara M, Tsuneoka-Suzuki T, Hashimoto Y, Enomoto T, Masuko T. Transformation of BALB3T3 cells caused by over-expression of rat CD98 heavy chain (HC) requires its association with light chain: mis-sense mutation in a cysteine residue of CD98HC eliminates its transforming activity. Int J Cancer 2000;87:311–316.
14. Nakamura E, Sato M, Yang H, Miyagawa F, Harasaki M, Tomita K, Matsuoka S, Noma A, Iwai K, Minato N. 4F2 (CD98) heavy chain is associated covalently with an amino acid transporter and controls intracellular trafficking and membrane topology of 4F2 heterodimer. J Biol Chem 1999;274:3009–3016.
15. Yanagida O, Kanai Y, Chairoungdua A, Kim DK, Segawa H, Nii T, Cha SH, Matsuo H, Fukushima J, Fukasawa Y, Tani Y, Taketani Y, et al. Human L-type amino acid transporter 1 (LAT1): characterization of function and expression in tumor cell lines. Biochim Biophys Acta 2001;1514:291–302.

16. Campbell WA, Sah DE, Medina MM, Albina JE, Coleman WB, Thompson NL. TA1/LAT-1/CD98 light chain and system L activity, but not 4F2/CD98 heavy chain, respond to arginine availability in rat hepatic cells. Loss of response in tumor cells. J Biol Chem 2000; 275:5347–54.
17. Samnick S, Bader JB, Hellwig D, Moringlane JR, Alexander C, Romeike BF, Feiden W, Kirsch CM. Clinical value of iodine-123-α-methyl-L-tyrosine single-photon emission tomography in the differential diagnosis of recurrent brain tumor in patients pretreated for glioma at follow-up. J Clin Oncol 2002;20:396–404.
18. Kuwert T, Probst-Cousin S, Woesler B, Morgenroth C, Lerch H, Matheja P, Palkovic S, Schafers M, Wassmann H, Gullotta F, Schober O. Iodine-123–methyltyrosine in gliomas: correlation with cellular density and proliferative activity. J Nucl Med 1997;38:1551–5.
19. Kaschten B, Stevenaert A, Sadzot B, Deprez M, Degueldre C, Del Fiore G, Luxen A, Reznik M. Preoperative evaluation of 54 gliomas by PET with fluorine-18-fluorodeoxyglucose and/or carbon-11-methionine. J Nucl Med 1998;39:778–85.
20. Langen KJ, Bonnie R, Muhlensiepen H, Jansen P, Broer S, Holschbach M, Coenen HH. 3-[123I]iodo-α-methyl-L-tyrosine transport and 4F2 antigen expression in human glioma cells. Nucl Med Biol 2001;28:5–11.
21. Shikano N, Kanai Y, Kawai K, Ishikawa N, Endou H. Characterization of 3-[125I]iodo-α-methyl-L-tyrosine transport via human L-type amino acid transporter 1. Nucl Med Biol 2003;30:31–7.
22. Langen KJ, Roosen N, Coenen HH, Kuikka JT, Kuwert T, Herzog H, Stocklin G, Feinendegen LE. Brain and brain tumor uptake of L-3-[123I]iodo–methyl tyrosine: competition with natural L-amino acids. J Nucl Med 1991;32:1225–8.
23. Storey BT, Fugere C, Lesieur-Brooks A, Vaslet C, Thompson NL. Adenoviral modulation of the tumor-associated system L amino acid transporter, LAT1, alters amino acid transport, cell growth and 4F2/CD98 expression with cell-type specific effects in cultured hepatic cells. Int J Cancer 2005;117:387–97.

Available online at www.sciencedirect.com
ScienceDirect
Biochimica et Biophysica Acta 1762 (2006) 673–682
BIOCHIMICA ET BIOPHYSICA ACTA
BBA
www.elsevier.com/locate/bbadis

Renal elimination of p-aminohippurate (PAH) in response to three days of biliary obstruction in the rat. The role of OAT1 and OAT3

Anabel Brandoni [a], Naohiko Anzai [b], Yoshikatsu Kanai [b], Hitoshi Endou [b], Adriana Mónica Torres [a,*]

[a] *Farmacología. Facultad de Ciencias Bioquímicas y Farmacéuticas. Universidad Nacional de Rosario. CONICET. Argentina*
[b] *Department of Pharmacology and Toxicology, Kyorin University School of Medicine, Tokyo, Japan*

Received 27 March 2006; received in revised form 24 May 2006; accepted 27 May 2006
Available online 7 June 2006

Abstract

Pharmacokinetic studies of the drugs administered to subjects with mechanical cholestasis are scarce. The purpose of the present study was to examine the effects of bile duct ligation of 3 days (peak of elevation of serum bile acids and bilirubin) on the systemic and renal PAH clearance and on the expression of cortical renal OAT1 and OAT3 in a rat model. PAH is the prototypical substrate of the renal organic anion transport system. Male Wistar rats underwent a bile duct ligation (BDL rats). Pair-fed sham-operated rats served as controls. BDL rats displayed a significantly lower systemic PAH clearance. Renal studies revealed a reduction in the renal clearance and in the excreted and secreted load of PAH in BDL rats. The OAT1 protein expression in kidney homogenates was not modified, but it decreased in the basolateral membranes from BDL rats. In contrast, OAT3 abundance in both kidney cortex homogenates and in basolateral membranes increased by 3 days after the ligation. Immunocytochemical studies (light microscopic and confocal immunofluorescence microscopic analyses) confirmed the changes in the renal expression of these transport proteins. The present study demonstrates the key role of OAT1 expression in the impaired elimination of PAH after 3 days of obstructive cholestasis.

Keywords: p-aminohippurate; Cholestasis; Renal depuration; OAT1; OAT3

1. Introduction

Extrahepatic, mechanical cholestasis occurs in about 10% of all patients suffering from cholelithiasis and in the majority of neoplasms affecting the pancreas and the common bile duct [1]. Prolonged cholestasis may alter the liver function due to an impaired uptake, changed biotransformation and secretion of compounds as well as secondary abnormalities induced within the kidney [2,3].

Pharmacokinetic studies of drugs administered to subjects with mechanical cholestasis are scarce [4]. Moreover, the obtained results are often conflicting, possibly due to the use of different species and interindividual differences.

The kidney and the liver play the major role in the elimination of numerous potentially toxic xenobiotics, including drugs, toxins, and endogenous metabolites. In some cases, the loss of one route of elimination can be compensated by the other [5]. It must also be mentioned that the impairment of liver or kidney functions can cause syndromes characterized by an injury of the alternative elimination organ [6,7].

In human beings and rats, extrahepatic cholestasis has been shown to render the kidney susceptible to a variety of nephrotoxic agents [6]. The pathophysiological cause of renal damage in the course of bile flow impairment is still not well understood, even though several phenomena, such as increased access of various constituents into the kidney (bilirubin and bile salts) have been suggested [6,7].

An impairment of the kidney function produces modifications in the renal elimination of drugs mediated by alterations in the blood flow to the kidney, glomerular filtration, active tubular secretion and passive tubular reabsorption [8].

The renal organic anion transport plays a critical role in protecting against the toxic effects of anionic substances, whether of

* Corresponding author. Suipacha 531, Rosario 2000, Argentina. Tel.: +54 341 4373787; fax: +54 341 4371992.
E-mail address: adtorres@fbioyf.unr.edu.ar (A.M. Torres).

0925-4439/$ - see front matter © 2006 Elsevier B.V. All rights reserved.
doi:10.1016/j.bbadis.2006.05.011

endogenous or environmental origin, by removing such substances from the blood principally via the organic anion transporter mechanisms found in the apical and basolateral membrane of renal epithelial cells. Several carrier proteins have been cloned and are functionally characterized from both membrane domains of rat kidneys [9–11]. The organic anion transporter 1 (OAT1) and the organic anion transporter 3 (OAT3) support the exchange organic anion/dicarboxylate transport in the basolateral membranes from the proximal tubule cells [12–15]. Two members of the multidrug resistance protein (MRP) family are located at the apical membranes from the proximal tubule cells, MRP2 and MRP4 [10,11,16,17]. The above mentioned four proteins mediate the renal transport of several anionic substances, such as p-aminohippurate (PAH), the prototypic organic anion commonly used in experimental studies. An up-regulation of renal MRP2 has been described at 1 and 3 days after bile duct ligation [18,19]. One day of bile duct ligation is referred as an early stage of obstructive cholestasis and 3 days of bile duct ligation is the period in which serum bile acids and bilirubin levels reach the peak of elevation [18–20]. MRP4 decreases at 3 days after bile duct ligation [21]. An increase in the urinary excretion of PAH has been concomitantly demonstrated with an increase in the abundance of OAT1 in the kidney homogenates in the early phase of an obstructive cholestasis [22].

The purpose of the present study was thus to examine the systemic and renal PAH clearance and the role of cortical renal OAT1 and OAT3 in response to 3 days of biliary obstruction in rats.

2. Materials and methods

2.1. Experimental animals

Male Wistar rats aged from 110 to 130 days old were used throughout the study (380–410 g body weight). In order to perform surgical procedures the animals were anaesthetized with sulfuric ether. After an upper abdominal incision was performed under sterile condition, the common bile duct was isolated and double-ligated close to the liver hilus immediately below the bifurcation and cut between the ligatures (BDL group). The controls then underwent a sham operation that consisted of exposure, but not a ligation, of the common bile duct (Sham group). The abdominal incision was then closed by single sutures. All studies were performed 3 days after surgery. All animals were allowed free access to a standard laboratory chow and tap water, and housed in a constant temperature and humidity environment with regular light cycles (12 h) during the experiment. All animals were cared for in accordance with the principles and guidelines for the care and use of laboratory animals [23].

2.2. Biochemical determinations

On the day of the experiment, blood was withdrawn from femoral artery of Sham and BDL animals. The serum was separated by centrifugation (3000 rpm, 3 min). These samples were used to measure total and direct bilirubin as parameters indicative of hepatic function and urea serum levels as a parameter indicative of global renal function. The above mentioned biochemical analyses were performed using optimized spectrophotometric techniques, while employing commercial kits (Wiener Laboratory).

2.3. Pharmacokinetic studies

These studies were done in a manner similar to those previously described [22,24]. At 3 days after surgery, the animals were anaesthetized with sodium thiopental (70 mg/kg b.w., i.p.). The femoral artery and the vein were both catheterized to obtain samples and to administer test compound, respectively. A single bolus of PAH (30 mg/kg b.w., aqueous solution, i.v.) was administered. Blood samples were obtained at 0–15 min range time after the administration of the PAH solution. The volume of blood samples was 50 μL. Eight blood samples were removed from each rat at different times between 0 and 15 min. An equivalent volume of isotonic saline solution was infused to restore the amount extracted in the blood samples. Samples were centrifuged at 3000 rpm for 3 min, and the extracted plasmas were frozen at −20 °C until analyzes.

At 15 min after PAH administration, a suprapubic incision was performed in order to isolate the bladder. Both ureters and the urethra were ligated with extreme care in order not to lose any urine. Thereafter, the bladder was removed and the whole contents of urine were then obtained to measure the quantity of PAH.

The plasma concentration vs. time curves for PAH, for each individual animal, were fitted with the PKCALC computer program [25]. The data were fitted to a biexponential curve. The choice of the best fit was based on the determination of coefficient values (R^2) and F test [25,26]. All fits had R^2 values >0.9. The following equation was used to describe the biexponential concentration–time curves:

$$Cp = Ae^{-\alpha t} + Be^{-\beta t}$$

where Cp is PAH plasma concentration (mg/mL) at time t (min) after administration; constant α represents the distribution from the central compartment and β is an equilibrium constant reflecting the dynamics between k_{21} and K_{10} and the slopes of each of the adjusted curves give their values. A and B represent the initial values of the distribution and elimination components, respectively, extrapolated from the y-axis intercept. The estimate parameters (α, β, A, B) were used to solve the first-order rate constants of transfer from the central to peripheral compartments (k_{12}, k_{21}) and the elimination rate constant from the central compartment (K_{10}) with classical equations. Derived parameters: area under curve (AUC), total volume of distribution (VdT), volume of the central compartment (VdC), volume of the peripheral compartment (VdP), steady-state volume of distribution (Vdss), systemic clearance (Cls), elimination half-life ($t_{1/2}$ β) were calculated according to standard procedures for the compartmental analysis. Cls was calculated as the Dose/AUC. The formulas for calculating the different volume of distribution were: VdT = Dose/[β × AUC], VdC = Dose/A + B, VdP = VdT − VdC, Vdss = Cls × MDRT, MDRT (mean disposition residence time) = AUMC/AUC, AUMC is the area under curve for the plot of the product of concentration and time vs. the time from time zero to infinity. Concentration of PAH in plasma and in urine was measured using the method described by Waugh and Beall [27].

2.4. Binding of PAH to plasma proteins

The binding of PAH to plasma proteins in Sham and BDL rats was determined using an ultrafiltration apparatus (Centrifree, Amicon, Millipore Corporation, Bedford, Mass) as previously described [24].

2.5. Renal excretion studies

These studies were performed as previously described [24,28–31]. Sham (n=4) and BDL (n=5) rats were anaesthetized as described. Femoral vein and artery were cannulated and a bladder catheter (3 mm i.d.) was inserted through a suprapubic incision. A priming dose of inulin (30 mg/kg b.w.) and PAH (30 mg/kg b.w.) in 1.5 mL of saline solution was administered through the venous catheter. Then, a solution containing inulin (12 g/L), PAH (12 g/L) and saline solution (9 g/L) was infused through the venous catheter employing a constant infusion pump (Pump 22; Harvard Apparatus, USA) at a rate of 1 mL/h/100 g b.w. After equilibrating for 45 min, urine was collected during two 20-min periods. Blood from the femoral artery was obtained at the midpoint of each clearance period. The arterial blood pressure was estimated throughout the experiments with a manometer inserted in the femoral artery. The glomerular filtration rate (GFR) was calculated from the clearance of inulin, in order to determine filtered load of PAH. The excreted, secreted and filtered loads of PAH were calculated by conventional formulae for each animal. The PAH concentrations in the serum and urine were determined by the method of Waugh and Beall [27] and the inulin concentrations were assayed by the procedure of Roe [32]. The volume of urine was determined by gravimetry.

2.6. Preparation of basolateral membrane (BLM) from kidney cortex

The preparations of BLM from Sham and BDL rats were done by a modification of the method described by Jensen and Berndt [33] as previously reported by

us [24,29]. Kidney cortical tissues were placed in a Dounce homogenizer containing 250 mM sucrose, 5 mM Tris–HEPES pH 7.40 at a ratio of 12.5 mL/g cortex wet weight. After four gentle strokes with the loose fitting pestle, the suspension was homogenized further with a motor-driven teflon pestle (600 rpm/5 strokes) and spun down for 15 min at 1200×g. The supernatant was aspirated and spun for 15 min at 22,000×g. The fluffy beige upper layer of the resulting pellet (crude plasma membranes) was resuspended in about 1 mL of supernatant and added to 19 mL of buffered sucrose. The membrane suspension was homogenized gently through a 16-gauge gavage needle followed by the addition of 3.7 mL of 100% Percoll. The Percoll-membranes mixture was spun for 30 min at 39,250×g. The top clear layer was discarded and the top-most dark band was removed. This layer was composed primarily of basolateral membranes. BLM were brought up in KCl buffer (85 mM KCl, 83 mM sucrose, 2 mM HEPES–Tris pH 7.40) at a ratio of 8 mL/g original cortex wet weight. Next, BLM were pelleted at 30,000×g for 30 min and washed three times with the KCl buffer. Finally, BLM were resuspended in 300 μL of 250 mM manitol, 10 mM HEPES–Tris, pH 7.40. Aliquots of the membranes were stored immediately at −70 °C until use (no more than 2 weeks after membrane preparations). Each preparation represents cortical tissue from four animals. Four preparations were obtained for each experimental group. Protein quantification of samples was performed using the method of Sedmak and Grossberg [34].

2.7. Electrophoresis and immunoblotting

Homogenates and basolateral membranes were boiled for 3 min in the presence of 1% 2-mercaptoethanol/2% SDS (Sodium Dodecyl Sulphate). Samples were applied to a 8.5% polyacrilamide gel, separated by SDS-PAGE, and then electroblotted to nitrocellulose membranes. Membranes were stained with Ponceau Red to confirm equal protein loading and transfer between lanes as previously described [21,22,28–30]. The nitrocellulose membranes were incubated with 5% nonfat dry milk in phosphate-buffer saline containing 0.1% Tween 20 (PBST) for 2 h. After being rinsed with PBST, the membranes were then incubated overnight at 4 °C with a commercial rabbit polyclonal antibody against rat OAT1 (1.25 μg/mL) and with commercial mouse monoclonal antibody against human β-Actin (1.25 μg/mL) or with non-commercial rabbit polyclonal antibody against rat OAT3 (at a dilution of 1:1000) and with commercial mouse monoclonal antibody against human β-Actin (1.25 μg/mL). The specificity of OAT3 antibody has been described elsewhere [15]. The membranes were incubated for 1 h with a peroxidase coupled goat anti-rabbit IgG (Bio-Rad) or with a peroxidase coupled sheep anti mouse IgG (Amersham) after further washing with PBST. Blots were processed for detection using commercial kit (Opti-4CN, Bio-Rad for OAT1 and ECL enhanced chemiluminescence system, Amersham for OAT3). To investigate the specificity of the bands, an absorption test was performed. The OAT1 peptide (1.25 μg/mL) or OAT3 peptide (0.50 mg/mL) were added to the OAT1-antibody specific solution or OAT3-antibody specific solution respectively and incubated for 2 h. Using these preabsorbed antibodies, Western blot analyses were performed as described above. A densitometric quantification of the Western blot signal intensity of membranes was performed.

Table 1
Pharmacokinetic parameters of PAH in Sham ($n=7$) and BDL ($n=8$) rats after a single dose (30 mg/kg b.w., i.v.)

	Sham	BDL
AUC (mg/min/mL)	0.88±0.04	1.34±0.15*
Cls (mL/min/100 g b.w.)	3.46±0.21	2.44±0.25*
A (mg/mL)	0.207±0.016	0.205±0.021
B (mg/mL)	0.095±0.016	0.087±0.013
α (min^{-1})	1.35±0.11	0.82±0.07*
β (min^{-1})	0.128±0.012	0.083±0.008*
K_{10} (min^{-1})	0.345±0.017	0.234±0.022*
k_{12} (min^{-1})	0.612±0.062	0.378±0.064*
K_{21} (min^{-1})	0.523±0.086	0.289±0.024*
$t_{1/2}$ (β) (min)	5.67±0.48	8.88±0.85*
VdT (mL/100 g b.w.)	28.43±2.79	31.12±4.37
VdC (mL/100 g b.w.)	10.11±0.55	10.50±0.59
VdP (mL/100 g b.w.)	18.32±2.52	20.61±4.16
Vdss (mL/100 g b.w.)	23.29±1.92	25.16±3.47

The results are expressed as the means±SEM. (*) $P<0.05$.
AUC=area under curve; Cls=systemic clearance; constant α represent the distribution from the central compartment and β is an equilibrium constant reflecting the dynamics between k_{21} and K_{10}; A and B represent the initial values of the distribution and elimination components, respectively; K_{10}=elimination constant from the central compartment; $t_{1/2}(\beta)$=elimination half-life ($t_{1/2}$); VdT=total volume of distribution; VdC=volume of the central compartment; VdP=volume of the peripheral compartment; Vdss=steady-state volume of distribution.

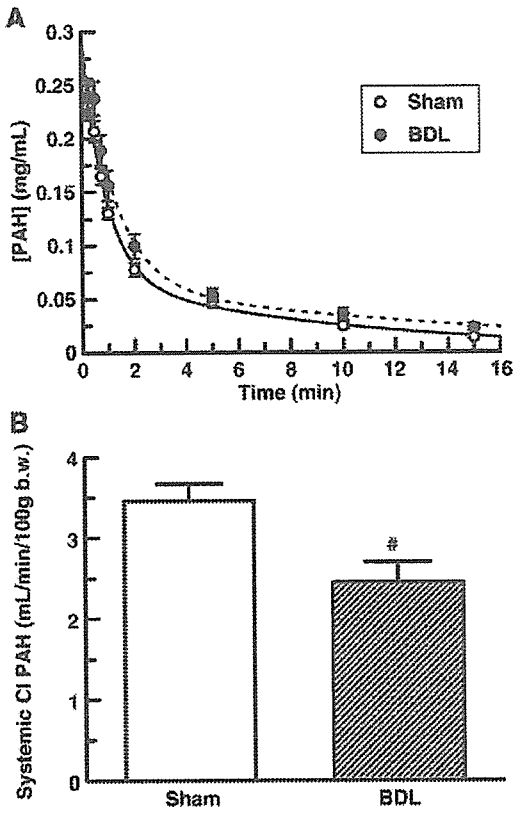

Fig. 1. Mean plasma concentration-time profile of PAH (A) and Systemic clearance of PAH (B) in Sham ($n=7$) and BDL ($n=8$) rats following a single 30 mg/kg b.w., i.v. dose of PAH. Results are expressed as the means±SEM. $^{\#}P<0.05$.

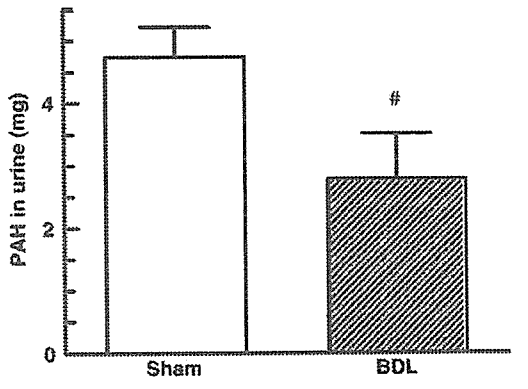

Fig. 2. Amount of PAH in urine excreted during 15 min following a single dose of PAH (30 mg/kg b.w., i.v.) in Sham ($n=7$) and BDL ($n=8$) animals. Results are expressed as the means±SEM. $^{\#}P<0.05$.

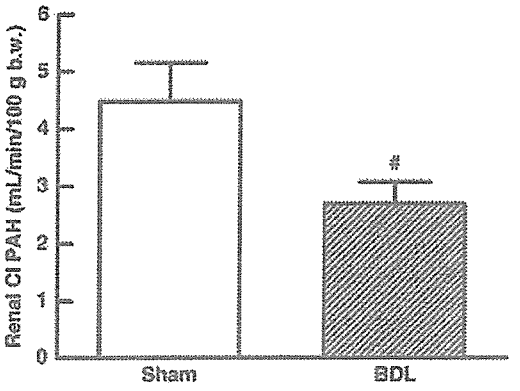

Fig. 3. Renal clearance of PAH in Sham ($n=4$) and BDL ($n=5$) rats. Results are expressed as the means±SEM. $^{\#}P<0.05$.

2.8. Immunocytochemistry microscopy

Kidneys from Sham and BDL rats were briefly perfused with saline, followed by perfusion with periodate–lysine–paraformaldehyde solution (0.01 M $NaIO_4$, 0.075 M lysine, 0.0375 M phosphate buffer, with 2% paraformaldehyde, pH: 6.20), through an abdominal cannula. The kidneys slices were immersed in periodate–lysine–paraformaldehyde solution at 4 °C overnight. The tissue was embedded in paraffin. Paraffin sections were cut. After deparaffining, the sections were incubated with 3% H_2O_2 for 15 min (to eliminate endogenous peroxidase activity) and then with blocking serum for 30 min. The sections were then incubated with non-commercial polyclonal antibodies against OAT1 (diluted 1:1000) or OAT3 (diluted 1:1000) overnight at 4 °C. The specificity of both antibodies has been described elsewhere [15]. The sections were rinsed with PBST.

2.9. Light microscopic analysis

The sections were incubated with biotinylated secondary antibody against rabbit Immunoglobulin for 1 h (biotinylated Ig Multi-Link Biogenex). After being rinsed with PBST, the sections were incubated for 30 min with horseradish peroxidase (HRP)-conjugated streptavidin solution (Streptavidin/HRP complex Multi-Link Biogenex). In order to detect HRP labeling a peroxidase substrate solution with diaminobenzidine (0.05% diaminobenzidine in PBST with 0.05% H_2O_2) was used. The sections were counterstained with hematoxylin before being examined under a light microscope.

2.10. Confocal microscopic analysis

The sections were incubated with Alexa 488 fluorochrome-conjugated goat anti-rabbit IgG, 1:1000 (Molecular Probes, Eugene, OR) overnight at 4 °C. Sections were washed with PBST and then mounted. Afterwards, they were viewed on a Zeiss Axiophot microscope equipped with an epifluorescence detector and a Bio-Rad MRC 1260 confocal imaging system.

Controls using preimmune serum, antiserum absorbed with excess synthetic peptide (as described above), or omission of primary or secondary antibody revealed no labeling.

Table 2
Body weight, kidneys weight, kidney/body weight ratio, plasma PAH concentrations (P_{PAH}), glomerular filtration rate (GFR), filtered, secreted and excreted loads of PAH (FL_{PAH}, SL_{PAH}, EL_{PAH}) in Sham ($n=4$) and BDL ($n=5$) rats

	Sham	BDL
Body weight (g)	342±18	367±7
Kidneys weight (g)	2.34±0.16	2.57±0.09
Kidney/Body weight ratio ($\times10^{-3}$)	6.84±0.26	6.99±0.16
P_{PAH} (μM)	295±28	376±63
GFR (mL/min/100 g b.w.)	0.858±0.074	0.515±0.058*
FL_{PAH} (μg/min/ 100 g b.w.)	40±4	35±5
SL_{PAH} (μg/min/ 100 g b.w.)	169±10	140±6*
EL_{PAH} (μg/min/100 g b.w.)	209±13	175±10*

The results are expressed as the means±SEM.
* $P<0.05$.

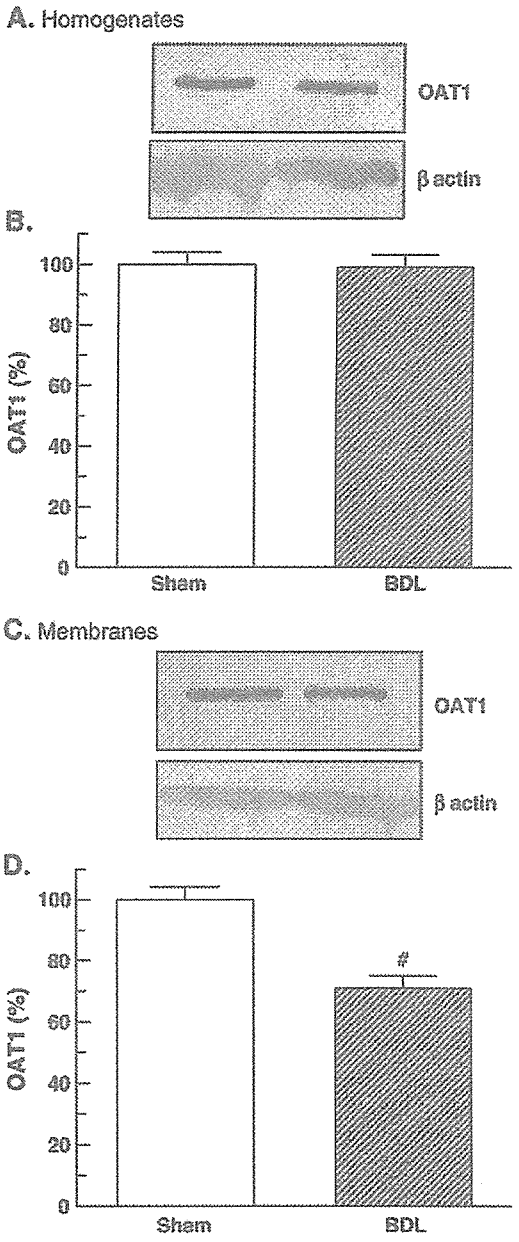

Fig. 4. Renal homogenates (50 μg proteins) (A) and basolateral membranes (40 μg proteins) (C) from kidneys of Sham and BDL rats were separated by sodium dodecyl sulphate-polyacrylamide gel electrophoresis (8.5%) and blotted onto nitrocellulose membranes. OAT1 was identified using commercial polyclonal antibodies as described in Materials and methods. Densitometric quantification of OAT1 Western immunoblotting from renal homogenates (B) and basolateral membranes (D). The results are expressed as percentage, normalized for the β actin density. The Sham levels were set at 100%. Each column represents the mean± SEM from experiments carried out in four different preparations for each experimental group. $^{\#}P<0.05$.

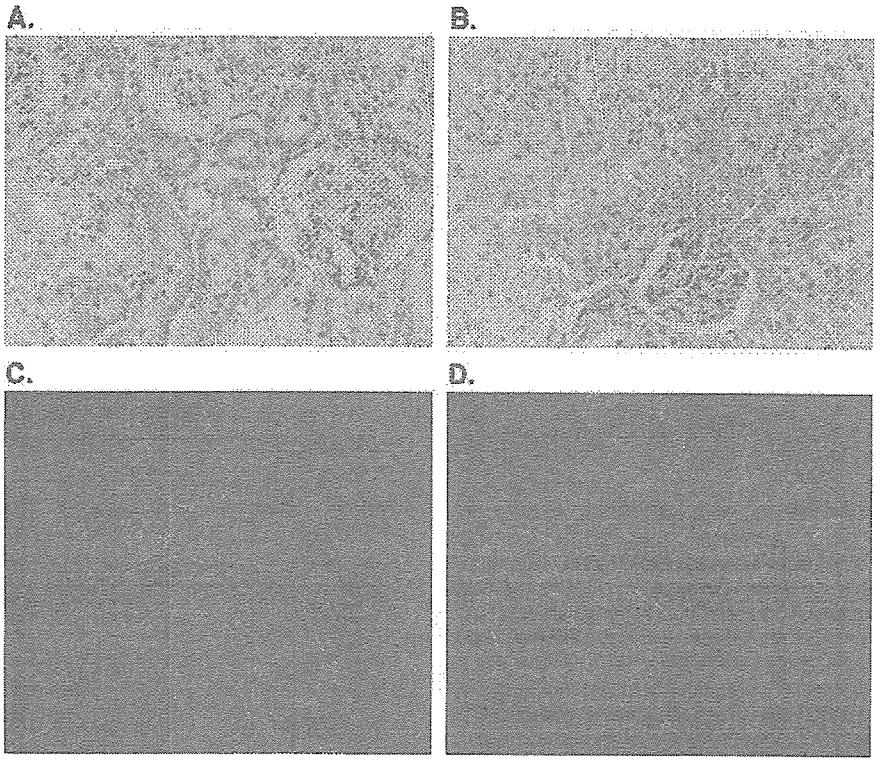

Fig. 5. Immunocytochemistry for OAT1. (A and B) Immunoperoxidase in the renal cortex of Sham (A) and BDL rats (B). Serial sections from each rat kidney were stained using a non-commercial anti-rOAT1 antibody (crude immune serum). OAT1 labeling was seen at the basolateral domains of proximal tubule cells. In BDL rats, it can be seen that OAT1 labeling in BLM is greatly reduced. These figures are representative of typical samples from four rats. Magnification ×400. (C and D) Immunofluorescence localization of OAT1 in the renal cortex of Sham (C) and BDL rats (D). Serial sections from each rat kidney were stained using a non-commercial anti-rOAT1 antibody (crude immune serum). In BDL rats, it can be seen OAT1 labeling throughout the cytoplasm in the proximal tubules, whereas the labeling of BLM was greatly reduced. These figures are representative of typical samples from four rats. Magnification ×400.

2.11. Histopathological studies

Histopathology of kidneys was performed after fixing in 10% neutral buffered formaldehyde solution for 4 h and embedding in paraffin, then 4 μm thick sections were processed for routine staining with hematoxylin and eosin, or stained with hematoxilin and PAS.

2.12. Materials

Chemicals were purchased from Sigma (St. Louis, MO, USA) and were analytical grade pure. The polyclonal antibodies against OAT1, monoclonal antibodies against β-actin and the OAT1 peptide for Western blotting were purchased from Alpha Diagnostic International (San Antonio, TX, USA). The polyclonal antibody against OAT1 for immunocytochemical studies and polyclonal antibody against OAT3 and the OAT3 peptide for both Western and immunocytochemical studies were non-commercial [15].

2.13. Statistical analysis

The statistical analysis was performed using the unpaired *t*-test. When variances were not homogeneous a Welch's correction was employed. *P* values of less than 0.05 were considered significant. The values are expressed as the means ± standard error (SEM). For these analyses, a GraphPad software was used. For densitometry of immunoblots, samples from kidneys of BDL rats were run on each gel with corresponding Sham kidneys. The abundance of OAT1 and OAT3 in the samples from the experimental animals was calculated as percentage of the mean Sham control value for that gel.

3. Results

Total bilirubin concentration in BDL rats increased to 71.34 ± 4.31 mg/L from 2.51 ± 0.36 mg/L observed in Sham group, whereas direct bilirubin level increased from 1.30 ± 0.24 mg/L in Sham animals to 66.85 ± 4.16 mg/L in BDL ones. Light microscopy only showed significant renal morphological alterations in PAS stained kidneys. In BDL rats, the kidney appears congestive, predominantly in the medulla. The tubular epithelium is less tall and shows apical extrusions and its foldings are less conspicuous. The cytoplasm presents a PAS (+) granularity. The tubules are moderately dilated, containing intraluminal proteinaceous, eosinophilic and acidophylic, material. These results are similar to those described by Wójcicki et al. [4].

On the other hand, no significant difference in the urea serum levels (g/L) was observed between the Sham-operated and BDL animals (0.40 ± 0.02 vs. 0.41 ± 0.02 respectively).

The mean plasma concentration-time profiles for PAH in Sham and BDL rats are shown in Fig. 1A. The higher plasma concentrations of PAH in BDL group were displayed during the distribution and elimination phases. BDL rats displayed a significant higher area under the curve and therefore a significant lower systemic clearance for PAH (Fig. 1B). The constant α (which represents the distribution from the central compartment),

the constant β (which is an equilibrium constant reflecting the dynamics between k_{21} and K_{10}), the rate constants of transfer from central to peripheral compartments (k_{12}, k_{21}) and the elimination rate constant from the central compartment (K_{10}) were all decreased in BDL rats, thus indicating the impairment in the rates of distribution and elimination of PAH (see Table 1). The distribution volumes were not significantly different between the Sham-operated and BDL animals as it is shown in Table 1.

A statistically significant decrease was observed in the quantity of PAH excreted in urine during 15 min (Fig. 2).

The percentage of unbound PAH to plasma proteins was higher in BDL rats than in the Sham ones (100±0.1 (n=4) vs. 95.3±1.4 (n=4), P<0.05, respectively). The values obtained for the Sham rats are similar to those previously reported [24].

Renal studies showed a decrease in the renal clearance of PAH in BDL rats as it is shown in Fig. 3. The excreted, secreted and filtered loads of PAH were lower in BDL rats compared with Sham rats, even though for the filtered load of PAH the difference did not reach the level of significance (Table 2). The glomerular filtration rate from jaundiced group was significantly lower in comparison with Sham group as it is also shown in Table 2. As a result, excreted load of PAH was lower in the BDL rats as consequence of the decrease in the secreted load of this organic anion.

Kidney cortex homogenates and basolateral membranes from Sham and BDL animals were subjected to immunoblot analyses for OAT1 protein. Fig. 4 shows no difference between the groups in the homogenates OAT1 expression. On the other hand, a lower abundance of OAT1 was observed in the basolateral membranes from BDL rats in comparison to the Sham rats. The OAT1 protein disappeared when the antibody was preabsorbed to the synthetic antigen peptide (data not shown).

Immunocytochemistry using horseradish peroxidase-conjugated secondary antibodies for light microscopy confirmed the reduced OAT1 expression in basolateral plasma membranes from BDL rats (Fig. 5B). The Sham rats showed an abundant OAT1 labeling in basolateral domains (Fig. 5A). To further characterize the distribution of OAT1 labeling in the proximal tubule cells, immunofluorescence was used (Fig. 5C and D). Confocal immunofluorescence studies also revealed a decrease in OAT1 labeling in basolateral plasma membranes and allowed a better appreciation of a punctuate labeling for OAT1, which was distributed widely throughout the cytoplasm in the kidneys from the BDL rats demonstrating the cellular internalization of this carrier protein.

The Western blotting findings of the kidney cortex homogenates and BLM from Sham and BDL rats showed signals for OAT3. In Fig. 6 it is possible to observe that the OAT3 abundance significantly increased in the kidney cortex homogenates and in the BLM from BDL rats in comparison to Sham ones. These signals were not observed when the antibody was preabsorbed with the OAT3 peptide (data not shown).

Immunocytochemistry studies showed staining for OAT3 in many parts of the nephron such as the proximal tubule (S1, S2 and S3), the distal and the collecting duct as it has been previously described [15]. Sham rats showed OAT3 labeling in basolateral membrane domain and inside the cytoplasm of renal tubular cells (Fig. 7A). Increased labeling was seen in the basolateral membranes of the tubules from kidneys of BDL rats (Fig. 7B). Immunofluorescence microscopy showed the basolateral membrane localization of OAT3 and a better detection of the intracellular localization (Fig. 7C). An important increase of OAT3 in basolateral membranes was observed in the cortex from

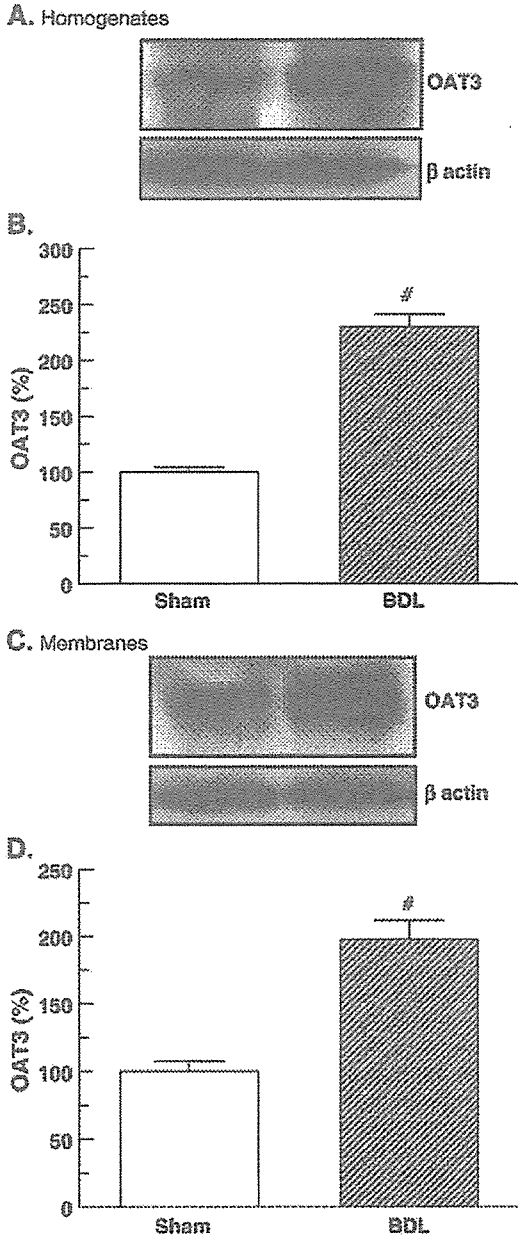

Fig. 6. Renal homogenates (50 μg proteins) (A) and basolateral membranes (40 μg proteins) (C) from kidneys of Sham and BDL rats were separated by sodium dodecyl sulphate-polyacrylamide gel electrophoresis (8.5%) and blotted onto nitrocellulose membranes. OAT3 was identified using non-commercial polyclonal antibodies as described in Materials and methods. The densitometric quantification of the OAT3 Western immunoblotting from renal homogenates (B) and basolateral membranes (D). Results are expressed as percentage, normalized for the β actin density. The Sham levels were set at 100%. Each column represents the mean±SEM from experiments carried out in four different membrane preparations for each experimental group. $^{\#}P<0.05$.

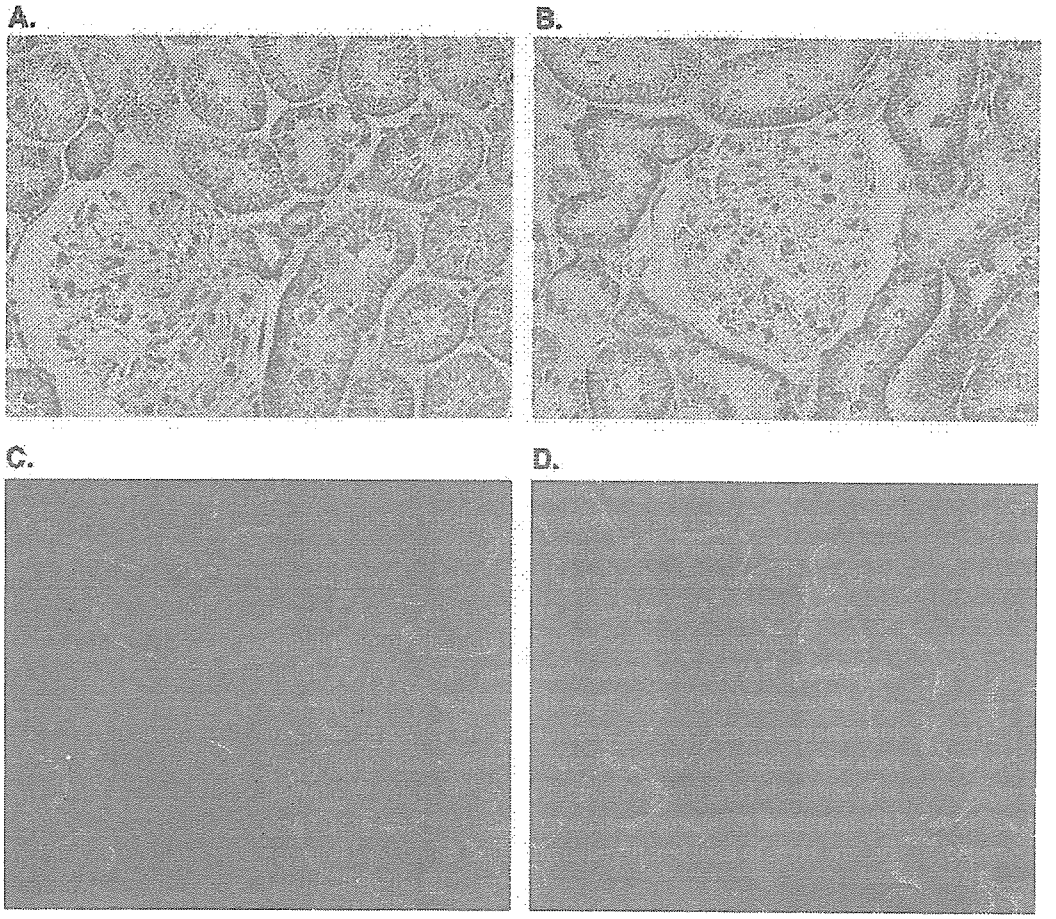

Fig. 7. Immunocytochemistry for OAT3. (A and B) Immunoperoxidase in the renal cortex of Sham (A) and BDL rats (B). Serial sections from each rat kidney were stained using a non-commercial anti-rOAT3 antibody. OAT3 labeling was seen at the basolateral domains of tubule cells and inside the cells. In BDL rats, it can be seen an increased OAT3 labeling in BLM. These figures are representative of typical samples from four rats. Magnification ×400. (C and D) Immunofluorescence localization of OAT3 in the renal cortex of the Sham (C) and BDL rats (D). Serial sections from each rat kidney were stained using a non-commercial anti-rOAT3 antibody. OAT3 labeling was seen at the basolateral domains of tubule cells and inside the cells. In the BDL rats, it could be seen as an increased OAT3 labeling in the BLM of tubular cells. These figures are representative of typical samples from four rats. Magnification ×400.

kidneys of BDL rats (Fig. 7D). This pattern parallels the data from an immunoblotting study.

4. Discussion

A large and diverse number of organic anions, or weak organic acids that exist as anions at physiological pH, are secreted by mammalian renal tubules. Substrates for the renal organic anion transport system include weak acids that have a net negative charge on carboxyl or sulfonyl residues at physiological pH [9–11]. Although this system secretes a number of endogenous compounds, it is generally accepted that is particularly important in secreting numerous exogenous compounds, including pharmacologically active substances, industrial and environmental toxins, and plant and animal toxins [9–11]. The transport of these substances across the basolateral membrane of renal epithelial cells is energetically uphill [9–11]. Molecular candidates for each of the organic anion transport process have been cloned, including OAT1 and OAT3 that serve as organic anion/dicarboxylate exchangers at the basolateral membrane of renal proximal tubule cells [9–15]. An unexplored aspect of OATs regulation concerns the body's response to disease states. We have recently demonstrated alterations in renal OAT1 and OAT3 expression in different experimental models in rats such as bilateral ureteral obstruction [28,29], arterial calcinosis [31], and chronic renal failure [30]. However, little is known about the regulation of these transporters after the early phase of extrahepatic cholestasis.

Acute jaundice due to bile duct obstruction is defined as the retention of bile and bile components. Biliary excretion of organic anions is a critical physiologic function of the liver. However, in obstructive jaundice, in which the biliary transport is impaired, adaptive mechanisms involving protein expression may permit urinary excretion of those potentially toxic compounds [1,4]. There are limited data on the pharmacokinetics of drugs in subjects with biliary obstruction.

Performing bile duct ligation as a well-established model of cholestasis, we have determined an increase in the systemic clearance of PAH associated to an increase in the abundance of OAT1 in renal cortex homogenates in rats at 21 h after bile duct ligation (early phase of acute extrahepatic cholestasis) [22]. The

aim of the present study was to examine the systemic and the renal clearance of PAH and the expression of both OAT1 and OAT3 in homogenates and basolateral membranes from rat renal cortex after a period of 3 days of bile duct obstruction (it has been well documented that serum bile salts and bilirubin levels reach the peak of elevation after 3 days of ligation [18–20]).

The clearance of a drug may be defined in a general way as "a proportionality constant describing the relationship between a substance's rate of transfer, in amount per unit time, and its concentration, in an appropriate reference fluid" [35]. The current study shows that rats at 3 days after bile duct ligation exhibit an increase in the area under the PAH plasma concentration–time curve and therefore, a statistically different decrease in the total body clearance. Furthermore, the total body clearance can be expressed as the product of the elimination rate microconstant ($K_{1\text{-}0}$) from the central compartment and the volume of such compartment. This last parameter was not modified in rats with extrahepatic cholestasis. On the other hand, a decrease was observed in $K_{1\text{-}0}$ in bile duct ligated rats as compared with Sham ones. $K_{1\text{-}0}$ is influenced by variables that participate in the elimination of the drug from the central compartment, such as metabolization, renal and biliary excretion. As PAH metabolization and biliary excretion is negligible, the decrease of $K_{1\text{-}0}$ observed in treated animals indicates a lower renal elimination of this organic anion. In this connection, rats subjected to bile duct ligation for 3 days showed a diminished renal PAH clearance. The decrease in renal PAH elimination is accounted for the diminished secreted load of the drug, since the filtered load of PAH was not modified in the BDL group.

In this cholestatic model, the OAT1 expression significantly decreased in the basolateral membranes from kidneys after 3 days of bile duct ligation. In addition to immunoblotting, immunocytochemical techniques corroborates the decrease in the basolateral membranes expression of OAT1 together with a significantly enhanced immunocytochemical staining for OAT1 in the cytoplasm of proximal tubule cells of BDL kidneys, which might suggest an internalization of membrane transporters or an inhibition in the recruitment of preformed transporters into the membranes.

It has been demonstrated that OAT1, when heterologously expressed in oocytes or mammalian cells, is inhibited by more or less selective PKC activators [36,37]. In this connection, it was demonstrated by Wolff et al. [38] that PKC induces human OAT1 down-regulation through carrier retrieval from the cell membrane and it does not involve phosphorylation. It is well known that angiotensin II [39] modulates the renal proximal tubule function via activation of PKC. Although the role of the renin–angiotensin system in the BDL model remains controversial [7], some humoral factors including angiotensin II induced by the 3 days BDL may induce the activation of PKC. Moreover, bile acids and high bilirubin levels can activate PKC [40,41]. It has been demonstrated that 3 days of bile duct ligation is the period in which serum bile acids and bilirubin levels reach the peak of elevation. We therefore postulate that the peak of elevation of bile acids and bilirubin can also trigger PKC activation. This PKC activation may cause the phosphorylation of caveolin-2, which may induce internalization of caveolae with OAT1 protein anchored with caveolin as has been recently suggested by Kwak et. al. [42]. This OAT1 downregulation (30%) was associated with a concomitant decrease of renal and systemic PAH clearance (40% and 30% respectively). The medium PAH plasma concentrations reached during the renal clearance infusion studies were 295 μM and 376 μM for the Sham and BDL rats respectively. The OAT1 mediated uptake of PAH is saturable with apparent Michaelis constants ranging 15 to 70 μM for rat OAT1 [13]. Therefore, PAH concentrations that we obtained in our "in vivo" experiments were sufficiently higher than the reported Km of rat OAT1. The diminished secreted load of PAH measured under saturating conditions was in part account for the lower number of OAT1 protein units observed, by immunoblot technique, in basolateral plasma membranes from BDL kidneys. The opposite was observed in the early phase of extrahepatic cholestasis where an increase of 30% of OAT1 abundance was associated with a similar increase in PAH clearance [22]. The differences observed in OAT1 abundance between 21 and 72 h of bile duct ligation remain to be explained. The increased OAT1 abundance observed in the early phase of extrahepatic cholestasis suggests a transient up-regulation similar to those described for renal OCT1 in cholestatic rats [43]. Maybe, different levels of various cytokines and growth factors which may affect gene transcription might be involved [44].

In contrast with OAT1, OAT3 expression increased both in homogenates and BLM from BDL kidneys. OAT3 is found in various cells and in all parts of the nephron, whereas OAT1 is confined to proximal tubules. The human and rat OAT3 transport PAH with relatively high affinity (87 and 65 μM respectively) [14,45], similarly to OAT1. On the contrary, estrone sulfate, cholate, and taurocholate are substrates for OAT3 and not for OAT1 as it has been demonstrated using *Xenopus laevis* oocytes [12,14,45,46], MDCK cells [47] and OAT3 knockout mice [48]. It is therefore possible that the over-expression of OAT3 does not compensate for the down-regulation of OAT1 regarding PAH transport because in this pathology the high plasma levels of bile acids might compete with PAH for OAT3 transport. Moreover, bile acids have been shown to regulate the expression of several genes involved in bile salt transport [49–51]. It is possible that high bile acids levels up-regulate OAT3 expression without affecting the OAT1 expression, being this another example of substrate specific regulation. The up-regulation of OAT3 protein in rat kidney in the present study is thus consistent with the adaptation to increased plasma bile acid levels that result from obstructive cholestasis, thus providing an additional alternative pathway for bile salt elimination.

MRP2 up-regulation has been described in the kidneys from rats with bile duct obstruction of 1 and 3 days [18,19]. On the other hand, renal MRP4 was down-regulated at 3 days after biliary obstruction [21]. Therefore, the protein expression of the luminal (MRP2 and MRP4) and basolateral organic anions renal transporters (OAT1 and OAT3), which all transport PAH, are differently regulated in extrahepatic biliary obstruction, thus indicating that different roles are played by these transporters in the pathogenesis of cholestasis. Tubular secretion is a vectorial transcellular transport system consisting of basolateral entry into the epithelial cells and secretion across the brush border membranes. Defects in either of

these two processes should therefore influence the tubular secretion of ionic drugs. In the present study, the tubular secretion of PAH was markedly reduced, thus suggesting a predominant role of OAT1 in this process.

It is important to mention that to predict the efficacy of a drug in vivo, it is critical to account for plasma protein binding because it determines the availability of the free drug, its half-life, and its subsequent renal elimination. Bow et al. [52] recently demonstrated that the degree of binding affinity for albumin to substrate determines whether or not a compound is actively secreted or reabsorbed by organic anion transporters. The common high unbound fraction of PAH increased from 95% in Sham rats to 100% in BDL rats. Since the bile acids and bilirubin plasma levels significantly increased in this experimental model, hence the binding sites on albumin for such hydrophobic anions might thus be occupied in the jaundiced rat, thereby increasing even more the unbound fraction of PAH.

The increase in the unbound fraction of PAH in BDL rats did not modify the distribution volumes of this anion. Nevertheless, in BDL rats there is a higher free concentration of PAH available for organic anion transporters, the OAT1 downregulation leads to a decrease in renal and systemic PAH clearance, thereby again stressing the main role of OAT1 in PAH excretion.

The present study stresses, once more, the important role of OAT1 expression in the renal elimination of PAH, independently of renal OAT3 expression. In this connection, it has been reported that a decrease of OAT1 abundance in BLM is associated with a decrease in PAH renal elimination in chronic renal failure [30], in obstructive nephropathy [28,29] and in response to 3 days of bile duct ligation, as it is shown in the present study. Meanwhile, OAT3 abundance in renal BLM has not changed, decreased or increased, respectively, in these three experimental models of pathologies [28–30]. Moreover, the increased renal excretion of PAH and furosemide is concomitantly observed with an increase in OAT1 and no changes in OAT3 abundance in BLM from rats with an early stage of extrahepatic cholestasis [22,53]. Accordingly, Eraly et al. [54] recently reported, using the OAT1 knock out mouse model, that regardless of the potential contribution of OAT3, the bulk of organic anion transport during the basolateral uptake step of the classical pathway is mediated by OAT1.

As highly accumulated anionic drugs observed during cholestasis may cause general body deterioration, the molecular mechanism(s) involved in the differential renal regulation of MRP2, MRP4, OAT3 and OAT1 expression should therefore be elucidated to prevent the occurrence of drug-induced toxicity due to this pathology.

Acknowledgements

This study was supported by the following grants: FONCYT and CONICET. The authors thank to Prof. Juan C. Picena (Cátedra de Anatomía y Fisiología Patológicas, Facultad de Ciencias Médicas, U.N.R.) and to Mrs, Alejandra Martínez (Facultad de Ciencias Bioquímicas y Farmacéuticas, U.N.R.) for their contribution to the histological studies. The authors also thank Wiener Lab Argentina for analytical kits. AMT was recipient of a travel grant from CONICET/JSPS (Japan Society for the Promotion of Science).

References

[1] N.R. Koopen, M. Müller, R.J. Vonk, P. Zimniak, F. Kuipers, Molecular mechanisms of cholestasis: causes and consequences of impaired bile formation, Biochim. Biophys. Acta 1408 (1998) 1–17.
[2] J. Reichen, F.R. Simon, Cholestasis, in: M. Arias, W.B. Jakoby, H. Popper, D. Schachter, D.A. Shafritz (Eds.), The Liver: Biology and Pathobiology, 2nd ed., Raven Press, New York, 1988, pp. 1105–1124.
[3] H.J. Kramer, Impaired renal function in obstructive jaundice: roles of the thromboxane and endothelin systems, Nephron 77 (1997) 1–12.
[4] M. Wójcicki, M. Drozdzik, T. Sulikowski, J. Wójcicki, B. Gawronska-Szklarz, S. Zielinski, L. Rózewicka, Pharmacokinetics of intravenously administered digoxin and histopathological picture in rabbits with experimental bile duct obstruction, Eur. J. Pharm. Sci. 11 (2000) 215–222.
[5] Ch. Fleck, H. Bräunlich, Interrelationships between excretion of drugs via urine and bile, Prog. Pharmacol. Clin. Pharmacol. 8 (1991) 511–529.
[6] M. Orellana, R. Rodrigo, L. Thielemann, V. Guajardo, Bile duct ligation and oxidative stress in the rat: effects in liver and kidney, Comp. Biochem. Physiol., Part C Pharmacol. Toxicol. 126 (2000) 105–111.
[7] S. Holt, R. Marley, B. Fernando, D. Harry, R. Anand, D. Goodier, K. Moore, Acute cholestasis-induced renal failure: effects of antioxidants and ligands for the thromboxane A2 receptor, Kidney Int. 55 (1999) 271–277.
[8] R. Talbert, Drug dosing in renal insufficiency, J. Clin. Pharmacol. 34 (1994) 99–110.
[9] N. Anzai, P. Jutabha, Y. Kanai, H. Endou, Integrated physiology of proximal tubular organic anion transport, Curr. Opin. Nephrol. Hypertens. 14 (2005) 472–479.
[10] T. Sekine, H. Miyazaki, H. Endou, Molecular physiology of renal organic anion transporters, Am. J. Physiol. 290 (2006) F251–F261.
[11] S.H. Wright, W.H. Dantzler, Molecular and cellular physiology of renal organic cation and anion transport, Physiol. Rev. 84 (2004) 987–1049.
[12] D.H. Sweet, L.M.S. Chan, R. Walden, X. Yang, D.S. Miller, J.B. Pritchard, Organic anion transporter 3 (Slc22a8) is a dicarboxylate exchanger indirectly coupled to the Na gradient, Am. J. Physiol. 284 (2003) F763–F769.
[13] T. Sekine, N. Watanabe, M. Hosoyamada, Y. Kanai, H. Endou, Expression cloning and characterization of a novel multispecific organic anions transporter, J. Biol. Chem. 272 (1997) 18526–18529.
[14] S.H. Cha, T. Sekine, J.-I. Fukushima, Y. Kanai, Y. Kobayashi, T. Goya, H. Endou, Identification and characterization of human organic anion transporter 3 expressing predominantly in the kidney, Mol. Pharmacol. 59 (2001) 1277–1286.
[15] R. Kojima, T. Sekine, M. Kawachi, S.H. Cha, Y. Suzuki, H. Endou, Immunolocalization of multispecific organic anion transporters, OAT1, OAT2, and OAT3, in rat kidney, J. Am. Soc. Nephrol. 13 (2002) 848–857.
[16] I. Leier, J. Hummel-Eisenbeiss, Y. Cui, D. Keppler, ATP-dependent para-aminohippurate transport by apical multidrug resistance protein MRP2, Kidney Int. 57 (2000) 1636–1642.
[17] P.H. Smeets, R.A. van Aubel, A.C. Wouterse, J.J. van den Heuvel, F.G. Russel, Contribution of multidrug resistance protein 2 (MRP2/ABCC2) to the renal excretion of p-aminohippurate (PAH) and identification of MRP4 (ABCC4) as a novel PAH transporter, J. Am. Soc. Nephrol. 15 (2004) 2828–2835.
[18] Y. Tanaka, Y. Kobayashi, E.C. Gabazza, K. Higuchi, T. Kamisako, M. Kuroda, K. Takeuchi, M. Iwasa, M. Kaito, Y. Adachi, Increased renal expression of bilirubin glucuronide transporters in a rat model of obstructive jaundice, Am. J. Physiol. 282 (2002) G656–G662.
[19] J. Lee, F. Azzaroli, L. Wang, C.J. Soroka, A. Gigliozzi, K.D.R. Setchell, W. Kramer, J.L. Boyer, Adaptive regulation of bile salt transporters in kidney and liver in obstructive cholestasis in the rat, Gastroenterology 121 (2001) 1473–1484.
[20] Q.-L. Pei, Y. Kobayashi, Y. Tanaka, Y. Taguchi, K. Higuchi, M. Kaito, N. Ma, R. Semba, T. Kamisako, Y. Adachi, Increased expression of multidrug resistance-associated protein 1 (mrp1) in hepatocyte basolateral membrane and renal tubular epithelia after bile duct ligation in rats, Hepatol. Res. 22 (2002) 58–64.

[21] G.U. Denk, C.J. Soroka, Y. Takeyama, W.-S. Chen, J.D. Schuetz, J.L. Boyer, Multidrug resistance-associated protein 4 is up-regulated in liver but down-regulated in kidneys in obstructive cholestasis in the rat, J. Hepatol. 40 (2004) 585–591.
[22] A. Brandoni, N.B. Quaglia, A.M. Torres, Compensation increase in organic anion excretion in rats with acute biliary obstruction: Role of the renal organic anion transporter 1, Pharmacology 68 (2003) 57–63.
[23] National Institutes of Health, Guide for Care and Use of Laboratory Animals, Publication 86-23, National Institutes of Health, Bethesda, 1985.
[24] J.A. Cerrutti, N.B. Quaglia, A.M. Torres, Characterization of the mechanisms involved in the gender differences in p-aminohippurate renal elimination in rats, Can. J. Physiol. Pharm. 79 (2001) 805–813.
[25] R. Shumaker, A basic interactive computer program for statistical and pharmacokinetic analysis of data, Drug Metab. Rev. 17 (1986) 331–348.
[26] H. Motulsky, Using nonlinear regression to fit curves, in: H. Motulsky (Ed.), Intuitive Biostatistics, Oxford University Press, New York, 1995, pp. 227–283.
[27] W.H. Waugh, P.T. Beall, Simplified measurement of PAH and other arylamines in plasma and urine, Kidney Int. 5 (1974) 429–432.
[28] S.R. Villar, A. Brandoni, N.B. Quaglia, A.M. Torres, Renal elimination of organic anions in rats with bilateral ureteral obstruction, Biochim. Biophys. Acta 1688 (2004) 204–209.
[29] S.R. Villar, A. Brandoni, N. Anzai, H. Endou, A.M. Torres, Altered expression of rat renal cortical OAT1 and OAT3 in response to bilateral ureteral obstruction, Kidney Int. 68 (2005) 2704–2713.
[30] A.M. Torres, M. Mac Laughlin, A. Muller, A. Brandoni, N. Anzai, H. Endou, Altered renal elimination of organic anions in rats with chronic renal failure, Biochim. Biophys. Acta 1740 (2005) 29–37.
[31] N.B. Quaglia, A. Brandoni, A. Ferri, A.M. Torres, Early manifestation of nephropathy in rats with arterial calcinosis, Renal Failure 25 (2003) 355–366.
[32] H.H. Roe, A photometric method for determination of inulin in plasma and urine, J. Biol. Chem. 178 (1949) 839–844.
[33] R.E. Jensen, W.O. Berndt, Epinephrine and norephinephrine enhance p-aminohippurate transport into basolateral membrane vesicles, J. Pharmacol. Exp. Ther. 244 (1988) 543–549.
[34] J.J. Sedmak, S.E. Grossberg, A rapid, sensitive and versatile assay for protein using Coomassie Brilliant Blue G250, Anal. Biochem. 79 (1977) 544–552.
[35] G.R. Wilkinson, Clearance approaches in pharmacology, Pharmacol. Rev. 39 (1987) 1–47.
[36] R. Lu, B.S. Chan, V.L. Schuster, Cloning of the human kidney PAH transporter: Narrow substrate specificity and regulation by protein kinase C, Am. J. Physiol. 276 (1999) F295–F303.
[37] G. You, K. Kuze, R.A. Kohanski, K. Amsler, S. Henderson, Regulation of mOAT-mediated organic anion transport by okadaic acid and protein kinase C in LLC-PK1 cells, J. Biol. Chem. 275 (2000) 10278–10284.
[38] N.A. Wolff, K. Thies, N. Kuhnke, G. Reid, B. Friedrich, F. Lang, G. Burckhardt, Protein kinase C activation downregulates human organic anion transporter 1-mediated transport through carrier internalization, J. Am. Soc. Nephrol. 14 (2003) 1959–1968.
[39] Z. Karim, N. Defontaine, M. Paillard, J. Poggioli, Protein kinase C isoforms in rat kidney proximal tubule: acute effect of angiotensin II, Am. J. Physiol. 269 (1995) C134–C140.
[40] Y.-P. Rao, R.T. Stravitz, Z.R. Vlahcevic, E.C. Gurley, J.J. Sando, P.B. Hylemon, Activation of protein kinase C α and δ by bile acids: correlation with bile acid structure and diacylglycerol formation, J. Lipid Res. 38 (1997) 2446–2454.
[41] Y. Hirohata, M. Fujii, Y. Okabayashi, Y. Nagashio, M. Tashiro, I. Imoto, T. Akiyama, M. Otsuki, Stimulatory effects of bilirubin on amylase release from isolated rat pancreatic acini, Am. J. Physiol. 282 (2002) 242–256.
[42] J.O. Kwak, H.-W. Kim, K.-J. Oh, D.S. Kim, K.O. Han, S.H. Cha, Co-localization and interaction of organic anion transporter 1 with caveolin-2 in the kidney, Exp. Mol. Med. 37 (2005) 204–212.
[43] G.U. Denk, C.J. Soroka, A. Mennone, H. Koepsell, U. Beuers, J.L. Boyer, Down-regulation of the organic cation transporter 1 of rat liver in obstructive cholestasis, Hepatology 39 (2004) 1382–1389.
[44] L.A. Denson, A. Bohan, M.A. Held, J.L. Boyer, Organ-specific alterations in RARα:RXRα abundance regulate rat Mrp2 (Abcc2) expression in obstructive cholestasis, Gastroenterology 123 (2002) 599–607.
[45] H. Kusuhara, T. Sekine, N. Utsunomiya-Tate, M. Tsuda, R. Kojima, S.H. Cha, Y. Sugiyama, Y. Kanai, H. Endou, Molecular cloning and characterization of a new multispecific organic anion transporter from rat brain, J. Biol. Chem. 19 (1999) 13675–13680.
[46] Y. Uwai, M. Okuda, K. Takami, Y. Hashimoto, K. Inui, Functional characterization of the rat multispecific organic anion transporter OAT1 mediating basolateral uptake of anionic drugs in the kidney, FEBS Lett. 438 (1998) 321–324.
[47] A. Aslamkhan, U.-H. Han, R. Walden, D.H. Sweet, J.B. Pritchard, Stoichiometry of organic anion/dicarboxylate exchange in membrane vesicles from rat renal cortex and hOAT1-expressing cells, Am. J. Physiol. 285 (2003) F775–F783.
[48] D.H. Sweet, D.S. Miller, J.B. Pritchard, Y. Fujiwara, D.R. Beier, S.K. Nigam, Impaired organic anion transport in kidney and choroid plexus of organic anion transporter 3 (Oat3 (Slc22a8)) knockout mice, J. Biol. Chem. 30 (2002) 26934–26943.
[49] D. Rost, T. Herrmann, P. Sauer, H.-L. Schmidts, B. Stieger, P.J. Meier, W. Stremmel, A. Stiehl, Regulation of rat organic anion transporters in bile salt-induced cholestatic hepatitis: effect of ursodeoxycolate, Hepatology 38 (2003) 187–195.
[50] D. Jung, M. Podvinec, U.A. Meyer, D.J. Mangelsdorf, M. Fried, P.J. Meier, G.A. Kullak-Ublick, Human organic anion transporting polypeptide 8 promoter is transactivated by the farnesoid X receptor/bile acid receptor, Gastroenterology 122 (2002) 1954–1966.
[51] J.L. Boyer, M. Trauner, A. Mennone, C.J. Soroka, S.-Y. Cai, T. Moustafa, G. Zollner, J.Y. Lee, N. Ballatori, Up-regulation of a basolateral FXR-dependent bile acid efflux transporter, OSTα-OSTβ, in cholestasis in humans and rodents, Am. J. Physiol. 290 (2006) G1124–G1130.
[52] D.A. Bow, J.L. Perry, J.D. Simon, J.B. Pritchard, The impact of plasma protein binding on the renal transport of organic anions, J. Pharmacol. Exp. Ther. 316 (2006) 349–355.
[53] A. Brandoni, S.R. Villar, J.C. Picena, N. Anzai, H. Endou, A.M. Torres, Expression of rat renal cortical OAT1 and OAT3 in response to acute biliary obstruction, Hepatology 43 (2006) 1092–1100.
[54] S.A. Eraly, V. Vallon, D.A. Vaughn, J.A. Gangoiti, K. Richter, M. Nagle, J.C. Monte, T. Rieg, D.M. Truong, J.M. Long, B.A. Barshop, G. Kaler, S.K. Nigam, Decrease renal organic anion secretion and plasma accumulation of endogenous organic anions in OAT1 knock-out mice, J. Biol. Chem. 281 (2006) 5072–5083.

The PDZ domain protein PDZK1 interacts with human peptide transporter PEPT2 and enhances its transport activity

R Noshiro[1,2,4], N Anzai[1,4], T Sakata[1,2], H Miyazaki[1], T Terada[3], HJ Shin[1], X He[1], D Miura[1], K Inui[3], Y Kanai[1] and H Endou[1,2]

[1]*Department of Pharmacology and Toxicology, Kyorin University School of Medicine, Mitaka, Tokyo, Japan;* [2]*Fuji Biomedix Co. Ltd, Chuo-ku, Tokyo, Japan and* [3]*Department of Pharmacy, Kyoto University Hospital, Sakyo-ku, Kyoto, Japan*

The proton-coupled peptide transporter PEPT2 (*SLC15A2*) mediates the high-affinity low-capacity transport of small peptides as well as various oral peptide-like drugs in the kidney. In contrast to its well-characterized transport properties, there is less information available on its regulatory mechanism, although the interaction of PEPT2 to the PDZ (PSD-95, DgIA, and ZO-1)-domain protein PDZK1 has been preliminarily reported. To examine whether PDZK1 is a physiological partner of PEPT2 in kidneys, we started from a yeast two-hybrid screen of a human kidney cDNA library with the C-terminus of PEPT2 (PEPT2 C-terminus (PEPT2-CT)) as bait. We could identify PDZK1 as one of the positive clones. This interaction requires the PDZ motif of PEPT2-CT detected by a yeast two-hybrid assay, *in vitro* binding assay and co-immunoprecipitation. The binding affinities of second and third PDZ domains of PDZK1 to PEPT2-CT were measured by surface plasmon resonance. Co-immunoprecipitation using human kidney membrane fraction and localization of PEPT2 in renal apical proximal tubules revealed the physiological meaning of this interaction in kidneys. Furthermore, we clarified the mechanism of enhanced glycylsarcosine (Gly-Sar) transport activity in PEPT2-expressing HEK293 cells after the PDZK1 coexpression. This augmentation was accompanied by a significant increase in the V_{max} of Gly-Sar transport via PEPT2 and it was also associated with the increased surface expression level of PEPT2. These results indicate that the PEPT2–PDZK1 interaction thus plays a physiologically important role in both oligopeptide handling as well as peptide-like drug transport in the human kidney.

Kidney International (2006) **70,** 275–282. doi:10.1038/sj.ki.5001522; published online 31 May 2006

KEYWORDS: oligopeptides; oligopeptide transporter; PEPT2; PDZ; PDZK1

Correspondence: *Y Kanai, Department of Pharmacology and Toxicology, Kyorin University School of Medicine, 6-20-2 Shinkawa, Mitaka, Tokyo 181-8611, Japan. E-mail: ykanai@kyorin-u.ac.jp*

[4]These authors contributed equally to this work.

Received 6 August 2005; revised 21 February 2006; accepted 8 March 2006; published online 31 May 2006

Proton-coupled peptide transporters play an important role in the maintenance of nutrition by mediating the transport of di- and tripeptides across the brush border (apical) membranes of the small intestine and kidney. In addition, peptide transporters function as drug transporters for peptide-like drugs, including β-lactam antibiotics and angiotensin converting enzyme inhibitors.[1–3] Two proton-coupled oligopeptide transporters, PEPT1 and PEPT2, have previously been cloned in rabbits,[4–6] rats[7–9] and humans.[10–12] PEPT1 was thus shown to be a high-capacity, low-affinity transporter that is expressed mainly in small intestine and, to smaller extent, in kidneys. It has been shown to play an essential role in the absorption of small peptides arising from the digestion of dietary proteins. In contrast, PEPT2 was found to be a low-capacity, high-affinity transporter that is expressed in the kidneys. In rats, Pept1 and Pept2 are sequentially expressed: Pept1 is located in the early segment and Pept2 is in the late segment of the proximal tubules.[13] In addition, both Pept1 and Pept2 are localized in the apical membranes of renal proximal tubule in rats.[14,15] Although both transporters are expressed in the kidney, PEPT2 is thought to play a dominant role in the conservation of peptide-bound amino acids. Recently, Rubio-Aliaga *et al.*[16] have reported on the impaired renal reabsorption of peptide-bound amino acids in animals lacking Pept2.

Although the transport properties and characteristics of substrate recognition for PEPT2 have been well documented, there is less information available on PEPT2 regulation. Takahashi *et al.*[17] reported a pronounced upregulation of Pept2 mRNA and protein expression in 5/6 nephrectomized rats 2 weeks after surgery and the downregulation of its mRNA 16 weeks after surgery.[18] Wenzel *et al.*[19] demonstrated that the activation of signaling pathways involving protein kinase C changes the kinetic property of pig Pept2 in a renal cell line. Recently, Bravo *et al.*[20] demonstrated a strong inhibitory effect of EGF on the rat Pept2 transport capacity. However, the modulation of the PEPT2 function by its associated protein(s) still remains unclear.

In recent years, several PDZ domain proteins, such as NHERF1/EBP50, NHERF2/E3KARP, and PDZK1, have been identified in kidneys and thus have been suggested to be involved in the stabilization, targeting, and regulation of their binding partner.[21–24] The PDZ (PSD-95, DglA, and ZO-1)-binding domains have been identified in various proteins and they are considered to be modular protein–protein recognition domains that play a role in protein targeting and protein complex assembly.[25–27] This domain binds to proteins containing the tripeptide motif $(S/T)-X-\emptyset$ (X = any residue and $\emptyset$ = a hydrophobic residue) at their C-termini.[27] As Russel *et al.*[28] mentioned, PEPT2 is localized to the apical membrane and has C-terminal amino-acid sequences that match the PDZ-binding motif (T-K-L), in a manner similar to that of other apical organic anion transporters, such as MRP2/4, NPT1, Oatp1, Oat-k1/k2; thus, indicating that PEPT2 most likely binds to certain PDZ domain proteins. We have recently identified that the urate/anion exchanger URAT1, which has a PDZ motif at its C-terminus (T-Q-F), interacts with PDZK1.[29] Interestingly, both URAT1 and PEPT2 are expressed at the apical membrane of renal proximal tubules and they are considered to function in a reabsorptive pathway for endogenous organic anions (urate[30] and oligopeptides,[1–3] respectively). It is likely that these transporters bind to either the same or other PDZ domain protein(s) via its PDZ-motif.

Very recently, Kato *et al.*[31] examined the interaction between xenobiotic transporters including PEPT2, and PDZ proteins including PDZK1. PDZK1, originally identified as a protein that interacts with MAP17, a membrane-associated protein,[32] has been reported to interact with several membrane proteins through its PDZ domain.[33] Using coexpression of PEPT2 C-terminus (PEPT2-CT) and PDZK1 in yeast, a possible interaction was demonstrated in the artificial condition. Because they solely rely on data from *in vitro* binding assays and did not provide any evidence that this interaction truly occurs in proteins expressed from the endogenous tissue, we performed yeast two-hybrid screening against a human kidney cDNA library using PEPT2-CT as bait and thus characterized this interaction in order to identify PDZK1 as a physiological binding partner of PEPT2.

RESULTS

Identification of PDZK1 by yeast two-hybrid library screening

In an attempt to isolate PEPT2-interacting protein(s) from the endogenous genes, we performed yeast two-hybrid screening against a cDNA library constructed from the human adult kidney using the PEPT2-CT as bait. From the 8.7×10^6 transformants screened, we obtained 64 positive clones. One of these clones had a sequence identical to a portion of the human PDZK1 gene.[32] We could not detect any interactions between PEPT2-CT and any other PDZ proteins that are expressed at and/or beneath the apical membrane of proximal tubules including NHERF1/EBP50, NHERF2/E3KARP, and IKEPP[34–37] (data not shown).

C-terminal PDZ motif of PEPT2 is necessary for PDZK1 interaction

To identify the region of PEPT2 that interacts with PDZK1, we constructed three mutant baits. A bait (PEPT2-CTd3) which lacks the last three residues of PEPT2, which play a crucial role in PDZ domain recognition. Two other baits (L729A and T727A), the extreme C-terminal leucine (0 position) or threonine (−2 position) of PEPT2 was replaced by alanine, which was expected to abolish the PDZ interactions.[38] These three baits did not interact with PDZK1 (Figure 1a). Therefore, the binding through PEPT2-CT suggests that the PDZ motif of PEPT2 is the site of interaction with PDZK1.

The interaction specificity between PDZK1 and PEPT2-CT was confirmed by a yeast two-hybrid assay using a bait that had the C-terminus of another human peptide transporter, PEPT1. PDZK1 did not interact with PEPT1-CT which lacks a PDZ motif (K-Q-M) (Figure 1b).

Interaction of PDZK1 individual PDZ domains with PEPT2-CT

PDZK1 possesses four PDZ domains which facilitate the assembly of protein complexes when target proteins bind via their C-terminal PDZ motifs. To determine the possible interactions of PEPT2-CT with the PDZ domains of PDZK1, we produced prey vectors, with each containing one of the individual PDZ domains (PDZ domain 1 (PDZ1), PDZ2, PDZ3, and PDZ4) from PDZK1. The interaction with the

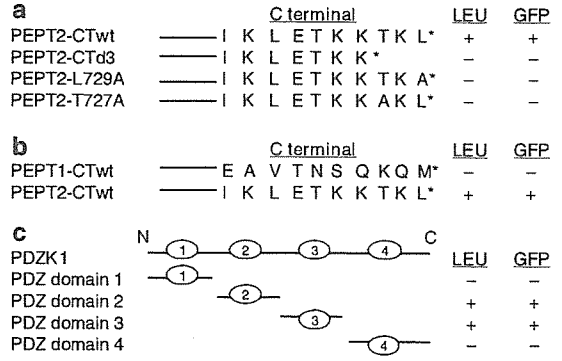

Figure 1 | Specificity of PDZK1 interaction with C-termini of PEPT2 in yeast two-hybrid system. (**a**) PDZK1 specifically interacted with the wt PEPT2 C-terminus but not with the C-terminal mutants L729A, T727A, and d727–729 (d3) of PEPT2. (**b**) Full-length PDZK1 interacting with the intracellular C-terminus of PEPT2 but not with that of PEPT1. (**c**) The wt PEPT2 C-terminus bait interacts with prey containing either the second or third PDZ domains of PDZK1 (PDZ2, PDZ3). The specificity of the prey containing a single PDZ domain of PDZK1 for the PEPT2 bait was confirmed by the absence of growth associated with the PEPT2 d3 mutant baits. The bars represent the approximate length of the baits, and the sequence of the last 10 amino acids is shown. pJG4-5 with PDZK1 cDNA expression cassette is under the control of the GAL1 promoter, such that library proteins are expressed in the presence of galactose (Gal) but not glucose (Glu). The system used for the yeast two-hybrid screen includes the reporter genes LEU2 and GFP, which replace the commonly used classical *lacZ* gene and allow a fast and easy detection of positive clones with long-wave UV. The results from the growth assay and GFP fluorescence are indicated on the right.

PEPT2-CT was observed for PDZ2 and PDZ3, but not for PDZ1 and PDZ4 of PDZK1 (Figure 1c).

In vitro binding of PEPT2 and PDZK1

We used a glutathione-*S*-transferase (GST) pull-down assay to confirm the ability of PEPT2-CT to bind to PDZK1 *in vitro* and validate the protein–protein interaction (Figure 2a). GST fusion proteins bearing the wild-type C-terminus (PEPT2-CT-wt) or C-terminal mutants (PEPT2-CTd3, L279A, and T727A) of PEPT2 were used to pull down *in vitro* translated full-length PDZK1. The data showed the same interaction specificity for PDZK1 and PEPT2 as exhibited in yeast two-hybrid assay (Figure 1a). As expected, the binding of PDZK1 to PEPT2 was completely abolished when the C-terminal PDZ motif was removed (PEPT2-CTd3) or mutated (PEPT2-CT-L729A or PEPT2-CT-T727A) (Figure 2a).

To confirm and quantify the interaction of PEPT2 with PDZK1, we performed surface plasmon resonance experiments using immobilized GST-PEPT2-CT and PDZ2 and PDZ3 of PDZK1 proteins independently fused to maltose-binding protein. As summarized in Table 1, the binding affinities of PDZ2 and PDZ3 of PDZK1 are low ($K_D = 10$ and 15 μM). These values are low in comparison to most PDZ domain interactions ($K_D = 1$ nM–10 μM).[39]

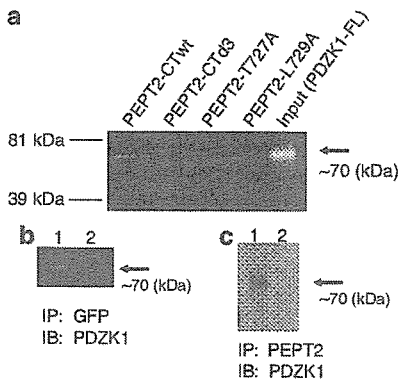

Figure 2 | Interaction of PDZK1 with PEPT2. (**a**) Full-length PDZK1 polymerase chain reaction product was *in vitro* translated in the presence of Transcend Biotinylated Lysine tRNA (Promega). The *in vitro* translation products were incubated with GST alone (lane 1), GST-PEPT2-CTwt (lane 2), or GST-PEPT2-CTd3 (lane 3) using a ProFound Pull-Down GST Protein:Protein Interaction kit (Pierce). The pull-down products were analyzed by sodium dodecyl sulfate-polyacrylamide gel electrophoresis. The input corresponds to the crude *in vitro* translation reaction. Positions of molecular mass standards are indicated on the right. GST fused to PEPT2 C-terminal wt can co-precipitate PDZK1, confirming the specificity found in the yeast two-hybrid system. The mutant form of PEPT2 in which the C-terminal PDZ recognition motif is removed is not able to precipitate PDZK1. (**b**) Co-immunoprecipitation of PEPT2 and PDZK1 in HEK293 cells. HEK293 cells were transfected with pEGFP-C2 vectors encoding PEPT2-wt (lane 1) or PEPT2-d3 (lane 2) with pcDNA3.1-PDZK1 and then immunoprecipitated with the anti-GFP antibody. Then, the immunoprecipitates were resolved by sodium dodecyl sulfate-polyacrylamide gel electrophoresis and probed with anti-PDZK1 antibodies. (**c**) Human kidney membrane fractions were immunoprecipitated with the anti-PEPT2 antibody (lane 1) and control immunoglobulin G (lane 2). The presence of PDZK1 in the immunoprecipitates was determined by Western blotting with the anti-PDZK1 antibody used in a previous study.[29]

Co-immunoprecipitation from heterologous cells and tissue

To demonstrate that PEPT2 and PDZK1 can also interact in mammalian cells, we used a previously prepared rabbit polyclonal antibody against PDZK1.[29] We coexpressed full-length human PEPT2 fused with green fluorescent protein (GFP) (GFP-PEPT2) and PDZK1 in human embryonic kidney (HEK)293 cells. Wild-type GFP-PEPT2 was co-immunoprecipitated with a GFP-specific antibody but GFP-PEPT2 which lacked the last three residues was not precipitated with PDZK1 (Figure 2b).

Furthermore, we demonstrated an association between endogenous PDZK1 and PEPT2 in human tissue by co-immunoprecipitating PEPT2 from human kidney membrane fractions using the anti-PDZK1 antibody, but not control immunoglobulin G (Figure 2c). This result is the evidence that observed interaction occurs between protein partners expressed from endogenous genes in kidneys.

Expression of PEPT2 in human kidney sections

In rats, Pept2 is present at the apical membrane of renal proximal tubules[14,15] and in humans, PDZK1 is reported to be expressed at the apical side of proximal tubular cells.[29,40] To determine whether PEPT2 and PDZK1 colocalize at the apical membrane of renal proximal tubules in humans, we carried out immunostaining of human serial kidney sections using anti-PEPT2 antibody.[41] Consistent with the previous reports, in the renal cortex, PEPT2 immunoreactivities were detected at the apical side of proximal tubular cells (Figure 3).

Table 1 | Characteristics of interaction between PEPT2 C-terminus and PDZK1 PDZ domains 2 and 3 (PDZ2 and PDZ3)

Construct	k_a (1/mM s)	k_d (1/min)	K_D (μM)
PDZK1-PDZ2	7.2×10^2	7.5×10^{-3}	10
PDZK1-PDZ3	3.6×10^2	5.5×10^{-3}	15

The kinetic characteristics of the interaction with immobilized GST-fused PEPT2 C-terminus with the second and third PDZ domains of PDZK1 (PDZ2 and PDZ3) fused with MBP measured by SPR methods are summarized. Association rate constants (k_a), dissociation rate constants (k_d), and equilibrium dissociation constants ($K_D = k_d/k_a$) are given.

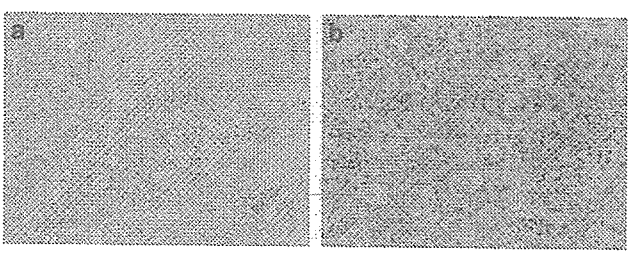

Figure 3 | Immunohistochemical analysis of PEPT2 in human kidney sections. (**a** and **b**) Immunohistochemical labeling of PEPT2 by diaminobenzidine reaction of human kidney. (**a**) PEPT2 was detected in proximal tubules in the cortex. (**b**) The apical membrane of proximal tubule was immunostained with the anti-hPET2 antibody and no immunostaining was observed in the basolateral membrane and glomeruli. These figures are representative of typical section samples. Original magnifications, (**a**) × 100 and (**b**) × 400.

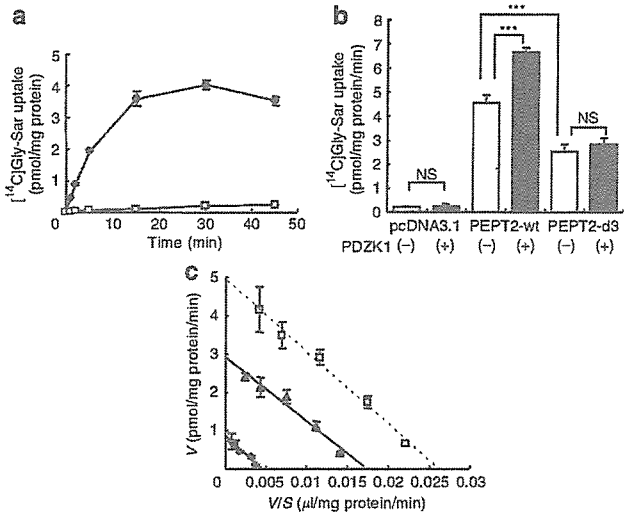

Figure 4 | Effect of PDZK1 on PEPT2-mediated [^{14}C]Gly-Sar transport activity. (a) The time profile of the uptake of [^{14}C]Gly-Sar via PEPT2. Intracellular accumulation of Gly-Sar was linear within 5 min and was significantly greater in PEPT2-wt-transfected HEK293 cells (HEK-PEPT2-wt; filled circles) than that in the mock-transfected cells (HEK-mock; open squares). (b) Coexpression of PEPT2 and PDZK1 increased [^{14}C]Gly-Sar uptake (30 μM) significantly over cells transfected with PEPT2 alone (closed column, middle). This effect was abolished when the C-terminal deletion mutant of PEPT2 was cotransfected with PDZK1 (HEK-PEPT2-d3; closed column, right), confirming that the interaction of PDZK1 with PEPT2 C-terminal domain is responsible for this effect. ***$P<0.001$ (c) Kinetic data using PEPT2-expressing HEK293 cells showed that PDZK1 (open squares) increased the V_{max} from 2.92 to 4.95 fmol/mg protein/min and increased the K_m slightly from 167 to 189 μM, as compared with PEPT2 alone (filled triangles). V_{max} of [^{14}C]Gly-Sar transport via HEK-PEPT2-d3 decreased (0.86 pmol/mg protein/min), whereas its K_m showed no change (187 nM) (filled circles). The kinetic parameters for the uptake via PEPT2 were estimated using $v = V_{max}[S]/(K_m + [S])$, where v is the uptake rate of substrates, $[S]$ is the substrate concentration (μM) in the medium. K_m is the Michaelis–Menten constant (μM) and V_{max} is the maximum uptake rate (pmol/mg of protein/2 min). These parameters were determined using the Eadie–Hofstee equation.

PEPT2 transport activity increases in presence of PDZK1

To determine whether PEPT2 and PDZK1 interaction is required to mediate the increase in PEPT2 transport activity, we transfected HEK293 cells with the pcDNA3.1(+) plasmid containing full-length PEPT2 (HEK-PEPT2-wt), PEPT2 lacking the last three amino acids (HEK-PEPT2-d3), or without an insert (HEK-mock). The time profile of the uptake of [^{14}C]glycylsarcosine (Gly-Sar) via PEPT2 is shown in Figure 4a. Intracellular accumulation of Gly-Sar was linear within 5 min and it was also significantly greater in HEK-PEPT2-wt than that in HEK-mock. After 2 min incubation, we demonstrated that [^{14}C]Gly-Sar uptake via HEK-PEPT2-wt was approximately 20-fold higher than that in HEK-mock and that in HEK-PEPT2-d3 was approximately 12-fold higher than that in HEK mock (Figure 4b). Gly-Sar transport activities significantly increased after PDZK1 coexpression (1.5-fold) (Figure 4b). This effect was not observed when PEPT2-d3 was coexpressed with PDZK1 (Figure 4b).

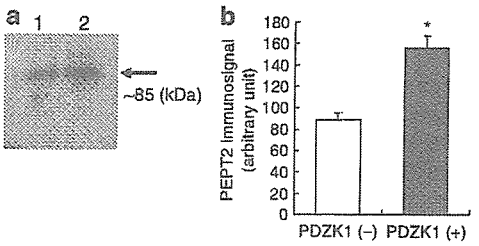

Figure 5 | Surface expression level of PEPT2. (a) cell surface biotinylation analysis of PEPT2 transiently expressing HEK293 cells transfected with vector alone (lane 1), and those transfected with PDZK1 (lane 2). Single bands of approximately 85 kDa, which are consistent with PEPT2, were observed in both lanes. (b) Quantification of immunosignal for PEPT2 ($n = 3$, error bars are s.d.). Densitometric analysis was performed using Model DIANA II Imaging System (M&S Instruments Trading Inc., Tokyo, Japan). *$P<0.05$.

Next, we examined the effect of PDZK1 coexpression on the kinetics of [^{14}C]Gly-Sar transport via HEK-PEPT2-wt that had been transfected with pcDNA3.1-PDZK1 or pcDNA3.1 alone. Kinetic data showed that PDZK1 significantly increased V_{max} from 2.92 to 4.95 pmol/mg protein/min and slightly increased K_m from 167 to 189 nM, in comparison to PEPT2 alone (Figure 4c). Interestingly, the V_{max} of [^{14}C]Gly-Sar transport via HEK-PEPT2-d3, decreased (0.86 pmol/mg protein/min), whereas its K_m showed no change (187 nM).

Surface expression level of PEPT2

To determine changes in the cell surface expression level of PEPT2, we used a cell-membrane-impermeant biotinylation reagent to selectively label the cell-surface proteins. After the treatment, the cell lysates from HEK293 cells transfected with PEPT2 and PDZK1 or PEPT2 and mock was collected. The amount of surface-biotinylated PEPT2 expression on plasma membranes increased 1.8-fold (PEPT2 and mock-transfected: 88.3 ± 6.9 vs PEPT2 and PDZK1-transfected: 155.5 ± 11.3 AU, $n = 3$) when PDZK1 was coexpressed (Figure 5). This change seems close to the one in V_{max} of PEPT2-mediated transport observed in Figure 4c.

DISCUSSION

The proton-coupled peptide transporter PEPT2 (*SLC15A2*) mediates the high-affinity low-capacity transport of small peptides in the kidney. Therefore, PEPT2 is presumed to contribute to the conservation of peptide-bound amino acids. Although the transport properties and characteristics of substrate recognition for PEPT2 have been well documented, there is less information on PEPT2 regulation. A recent report by Kato *et al.*[31] has provided the novel idea concerning the modulation of PEPT2 function by its associated protein. They demonstrated an interaction between the recombinant PEPT2 C-terminus fused to GST and purified His-tagged PDZK1, but they solely rely on data from *in vitro* binding assays and did not indicate the physiological importance of this interaction. In addition, the yeast two-hybrid screens performed by Gisler *et al.*,[42] using baits

containing single PDZ domains derived from mouse PDZK1, failed to detect Pept2 as a candidate for PDZK1 binding although several membrane proteins including Urat1 were found. To identify PDZK1 as a physiological binding partner of PEPT2, we evaluated this interaction from several viewpoints in this study.

Starting from a yeast two-hybrid screening of a human kidney cDNA library, we have demonstrated PDZK1 to be a physiological interactor of PEPT2. First, we could detect PDZK1 from 64 positive clones by library screening. Second, we could observe the co-immunoprecipitation of PEPT2 and PDZK1 from kidney membrane fractions (Figure 2c). Third, we could demonstrate the localization of PEPT2 protein at the apical side of the renal proximal tubules where PDZK1 is also expressed (Figure 3). These results indicate the physiological meaning of this interaction.

We have further examined this interaction by a yeast two-hybrid assay (Figure 1), an *in vitro* pull-down assay (Figure 2a), co-immunoprecipitation (Figure 2b) and surface plasmon resonance assay (Table 1) of recombinant proteins, as well as by the transport studies (Figure 4) and a cell surface biotinylation assay (Figure 5). These results support the preliminary data presented by Kato *et al.*[31] Moreover, the augmentation of the transport activity by PDZK1 was accompanied by a significant increase in the V_{max} of Gly-Sar transport via PEPT2 (Figure 4c) and was associated with the increased surface expression level of PEPT2 in HEK293 cells (Figure 5). These characteristics are closely similar to those of the URAT1–PDZK1 interaction,[29] and suggest PDZK1 to thus play a similar role in PEPT2–PDZK1 interaction; namely, that PEPT2 is stabilized and/or anchored at the cell membrane, making it less likely to be internalized and subsequently degraded.

Although their functional consequences are the same, there are several differences between the PEPT2–PDZK1 interaction and the URAT1–PDZK1 interaction. First, the frequency of PDZK1 appearing as a positive clones was smaller in the case of PEPT2 (one out of 64) than in the case of URAT1 (35 out of 98). Second, the interaction profiles of PDZK1 ligand against individual PDZ domains of PDZK1 were different, although they have similar C-terminal PDZ motifs: T-K-L for PEPT2 and T-Q-F for URAT1. PEPT2 binds to PDZ2 and PDZ3 (Figure 1), while URAT1 binds to PDZ1, PDZ2, and PDZ4.[29] Third, the binding affinities for each PDZ domain of PDZK1 were more than 10-fold lower for PEPT2 than for URAT1: 10 and 15 μM for PEPT2 (Table 1) and 1.97–514 nM for URAT1.[29] Fourth, when a C-terminal deletion mutant of URAT1 (URAT1-d3) was coexpressed with PDZK1, urate transport activity was not enhanced, but URAT1-d3 still demonstrated a similar urate transport activity to wt URAT1 when expressed without PDZK1. In contrast, the C-terminal deletion mutant of PEPT2 (PEPT2-d3) not only lacked the ability to enhance transport activity when coexpressed with PDZK1, but its transport activity was reduced to half that of the wt PEPT2 (PEPT2-wt) when expressed without PDZK1.

The low frequency of PDZK1 in PEPT2 screening seems consistent with the report of Gisler *et al.*[42] as we mentioned earlier in this paper. In addition to the expression levels of these proteins, the binding affinity is likely to affect the frequency of a particular protein appearing as a positive clone in yeast two-hybrid screening. Therefore, a low frequency of positive clone does not mean that the observed interaction is physiologically less important. Moreover, a low binding affinity may be advantageous for the regulatory dynamics of protein–protein interactions,[27] because a low binding affinity is related to an easier association and dissociation of proteins than a high binding affinity. In particular, PEPT2 has a putative protein kinase C (PKC) recognition site at its C-terminal close to the PDZ motif, whose phosphorylation may interfere with binding to the PDZ domain.[43] It will be interesting to investigate whether the phosphorylation of both PEPT2 and PDZK1 or either protein independently alters the binding affinity of this interaction, in order to clarify the regulatory mechanism for PDZ–ligand interaction.

The decreased transport activity of the PEPT2 C-terminal deletion mutant compared to wt PEPT2, together with the significant reduction in V_{max} (Figure 4) may indicate PDZ motif to thus play another role in the PEPT2-CT: the targeting of the transporter to the plasma membrane. This was originally predicted by Russel *et al.*[28] However, as mentioned above, this phenomenon was not observed in the C-terminal deletion mutant of URAT1 expressed in the same HEK293 cells that have endogenous PDZK1 at low level.[29] Although we frequently detected PDZK1 in the URAT1 screen, we did not find any other binding candidates for URAT1. In the PEPT2 screen, we detected several potential binding partners for PEPT2 besides PDZK1 (manuscript in preparation). It will therefore be important to identify other binding proteins surrounding PEPT2 to understand the potential significance of this interaction.

Recently, PDZ proteins have been recognized as orchestrating scaffolds to achieve concerted functions.[23] PEPT2 mediates an electrogenic proton-coupled cotransport that uses an inward proton gradient to transport small peptides from urine to the cell. Following the concept proposed by Moe, the ability of PDZK1 to couple PEPT2 to the Na^+/H^+ exchanger NHE3 may provide the necessary lumen-to-cell proton gradient, and the multimolecular protein complex will be functionally equivalent to a Na^+/oligopeptide cotransporter. A functional coupling between PEPT2 and NHE1 and/or NHE2 has recently been shown by Wada *et al.*[44] In this paper, we described, for the first time, the exact localization of PEPT2 in the human kidney in addition to its novel regulatory mechanism. PEPT2 proteins are expressed at the apical membrane of renal proximal tubules similarly to rat Pept1 and rat Pept2, which are expressed in the same site.[15] Based on the above findings, human PEPT2 may therefore be involved in the reabsorption of peptides on the apical side of the renal tubules, similar to that of rodent Pept2 and the protein complex surrounding PEPT2 should thus be clarified by identifying other interacting proteins to obtain a

Table 2 | PCR primers used in this study

Construct	Sense primer	Antisense primer
PEPT2-CTwt	5′-CGAATTCCTGCCCGAGACCCAGAG-3′	5′-CTCTCGAGCTAAAACTGTGTGGATTTTA-3′
PEPT2-CTd3	5′-CGAATTCCTGCCCGAGACCCAGAG-3′	5′-CCCTCGAGCTAGGATTTTAGGACAGAGTTC-3′
PEPT2-L727A	5′-CGAATTCCTGCCCGAGACCCAGAG-3′	5′-CCCTCGAGCTAAGCCTGTGTGGATTTTAGGA-3′
PEPT2-T729A	5′-CGAATTCCTGCCCGAGACCCAGAG-3′	5′-CCCTCGAGCTAAAACTGTGCGGATTTTA-3′

PCR, polymerase chain reaction; wt, wild type.

comprehensive understanding of the peptide transport function in the renal proximal tubules.

MATERIALS AND METHODS

Materials

[^{14}C]Glycosylsarcosine (Gly-Sar) (4 Ci/mmol) was obtained from Moravek (Brea, CA, USA). Other materials used included Ham F12 medium from Nissui Pharmaceutical Co., Ltd. (Tokyo, Japan), and fetal bovine serum and trypsin from Invitrogen (Carlsbad, CA, USA).

Cloning of human PEPT2 cDNA

The cDNA library was prepared from human kidney poly(-A)$^+$RNA.[45] The 0.46-kb cDNA fragment (24–481 nt of the nucleotide sequence of human PEPT2 (hPEPT2)) was obtained by polymerase chain reaction. This fragment was labeled with [^{32}P]dCTP (T7QuickPrime, Amersham Biosciences, Tokyo, Japan) and used as probe. The screening of the cDNA library was performed as described elsewhere.[46]

Plasmid construction

The C-terminal fragments of wt hPEPT2 cDNA and three mutants (designated d3, L729A, and T727A) were generated by polymerase chain reaction using specific primers (Table 2) and cloned into the *Bam*HI and *Xho*I sites of pEG202 (bait) and pGEX-6P-1 (Amersham Biosciences) to construct PEPT2-CTwt, PEPT2-CTd3, PEPT2-L729A, and PEPT2-T727A. The full-length coding sequences of hPEPT2 (wt) as well as its C-terminal 3-amino-acid-deletion mutant (d3) were inserted into the mammalian expression vector pcDNA3.1 (Invitrogen) for functional analysis and into pEGFP-C2 (Clontech, Tokyo, Japan) for GFP fusion protein preparation. The pcDNA3.1 vector containing the full-length human PDZK1 (hPDZK1) and preys (pJG4–5 and pMAL-C2x) containing single PDZ domains of hPDZK1 were prepared as described previously.[29]

Yeast two-hybrid assay

A human kidney cDNA library was constructed as described previously.[29] A PEPT2 C-terminal bait corresponding to the last 34 amino acids of PEPT2 was used to screen 8.7×10^6 clones of the human kidney cDNA library with the LexA-based GFP two-hybrid system (Grow'n' Glow system; MoBiTec, Göttingen, Germany).

In vitro binding assay

PEPT2-CT for GST fusion protein production in bacteria as reported previously.[47] *In vitro* translation was performed from a plasmid carrying the full-length PDZK1 with the TNT T7 Quick for polymerase chain reaction DNA system (Promega, Tokyo, Japan) in the presence of Transcend Biotinylated tRNA (Promega), as described elsewhere.[29] Of *in vitro*-translated products, (5 μl) was applied into ProFound™ Pull-Down GST Protein:Protein Interaction Kit (Pierce, Rockford, IL, USA) with 50 μl of GST-glutathione-Sepharose resin and protein complexes were eluted according to the manufacturer's instructions.

Surface plasmon resonance

The interactions of PEPT2-CT with the second and third PDZ domains of PDZK1 were investigated using a BIAcore 3000 analytical system (BIAcore AB, Tokyo, Japan). Using an amine coupling kit, GST-fused wt PEPT2-CT or GST alone was attached to a CM5 sensor chip according to the manufacturer's instructions, giving an increase of 11 214 resonance units (RU) for GST-PEPT2-CT or 8,566 resonance units for GST alone. Binding experiments were performed with the PDZK1 single PDZ domains fused with maltose-binding protein as described elsewhere.[29]

Immunohistochemical analysis

We used human single-tissue slides (Biochain, Hayward, CA, USA) for light microscopic immunohistochemical analysis as reported previously.[48] They were treated with 10 μg/ml primary rabbit polyclonal antibodies against PEPT2[41] or PDZK1 (4°C overnight).

Cell culture and transfection

HEK293 cells were maintained in Dulbecco's-modified Eagle's medium supplemented with 10% fetal bovine serum, 1 mM sodium pyruvate, penicillin (100 U/ml), and streptomycin (100 mg/ml) (Invitrogen) at 37°C in 5% CO_2. Transient transfection with Lipofectamine 2000 (Invitrogen, Gaithersburg, MD, USA) was performed according to the manufacturer's recommendations.

Immunoprecipitation and immunoblotting

Immunoprecipitation analysis was performed as described previously.[49] Lysates from HEK293 cells that expressed GFP-fused hPEPT2 and hPDZK1 were immunoprecipitated by the anti-GFP antibody (full-length A.v. polyclonal antibody, Clontech). For the co-immunoprecipitation of endogenous PEPT2 and PDZK1, we used human kidney membrane fractions (Biochain) and added the anti-PEPT2 antibody or control immunoglobulin G to this solution. After overnight incubation, PEPT2 and PDZK1 were immunoprecipitated using the Seize Classic (A) Immunoprecipitation kit (Pierce). The affinity-purified rabbit PDZK1 antibody and horseradish peroxidase-conjugated goat anti-rabbit immunoglobulin G (Amersham Biosciences) were used for immunoblotting with enhanced chemiluminescence reagents (ECL Plus, Amersham Biosciences).

Gly-Sar transport activity assay

HEK293 cells were plated on 24-well culture plates at a density of 2×10^5 cells/well 24 h prior to transfection, and they were transfected as described above. After 36 h, the culture medium was removed, and the cells were washed three times and incubated in